Fabrication and Characterization of Nano Probes for Scanning Electrochemical Microscopy

by

Hui Xiong

B.E., East China University of Science and Technology, 1998

Submitted to the Graduate Faculty of

School of Arts and Sciences in partial fulfillment

of the requirements for the degree of

Master of Science

University of Pittsburgh

2006

UNIVERSITY OF PITTSBURGH

School of Arts and Sciences

This thesis was presented

by

Hui Xiong

It was defended on

December 3, 2004

and approved by

Shigeru Amemiya, Assistant Professor, Department of Chemistry

Stephen G. Weber, Professor, Department of Chemistry

Adrian Michael, Associate Professor, Department of Chemistry

Thesis Director: Shigeru Amemiya, Assistant Professor, Department of Chemistry

Fabrication and Characterization of Nano Probes for Scanning Electrochemical Microscopy

Hui Xiong, M.S.

University of Pittsburgh, 2006

Selectively etched optical fibers were used as a template for fabrication of ultramicroelectrodes (UME), which are suitable for use as a probe in scanning electrochemical microscopy (SECM). Multistep index optical fibers with high-GeO_2-doped core and two cladding layers were chemically etched to a sharp point (10 nm in diameter) in NH_4F/HF buffer solutions. The etched fibers had a defined geometry and the etching process was highly reproducible. After etching, a layer of gold was sputtered on the fibers. The Au-coated fibers were then insulated by electrophoretic paint. The size and shape of the electrodes were determined by steady-state cyclic voltammetry and SECM. The SECM tip current-distance (approach) curves over conductive and insulating substrates agreed with the theoretical curves obtained by numerical simulations, which proves a conical electrode geometry. The base radius and height of the conical electrodes determined by SECM were in the range of 0.255-1.0 and 0.3-1.2 μm, respectively.

In order to fabricate electrodes within 200 nm in radius using selectively etched optical fiber as the template, we tried several approaches: (1) Using focused ion beam (FIB) milling we could cut the gold-coated tip at desired size with nanometer precision. However, after electrophoretic paint deposition on FIB modified fibers, the apparent size of the electrode increased against our expectation from FIB, which indicated that gold exposed not only at the tip but also on the side-wall. (2) Insulating gold-coated probes by sputtering silicon oxide has been investigated.

TABLE OF CONTENTS

1.0 INTRODUCTION 1

1.1 FAST AND LOCAL CHEMICAL REACTIONS AT BIOLOGICAL MEMBRANES 1

1.2 SCANNING ELECTROCHEMICAL MICROSCOPY (SECM) 2

1.3 EFFECT OF TIP GEOMETRY 5

1.4 FABRICATIONS OF PROBES FOR SECM 8

1.4.1 Disk-in-glass Microelectrode 8

1.4.2 Submicrometer Glass-Encapsulated Microelectrodes 9

1.4.3 Electrochemical Etching of Metal Wires and Insulation by Electrophoretic Paint 10

1.4.4 Self-assembled Spherical Gold UME 10

1.4.5 Ring Microelectrode by Focuses Ion Beam (FIB) 11

1.5 DESIGN AND CONSTRUCTION OF SUB-MICROMETER PROBES FOR SECM 11

1.5.1 Selectively Etched Optical Fibers 11

1.5.2 Electrophoretic Paint Technique 13

1.5.3 FIB Milling 13

1.6 REFERENCES 14

2.0 FABRICATION AND CHARACTERIZATION OF CONICAL MICROELECTRODE PROBES TEMPLATED BY SELECTIVELY ETCHED OPTICAL FIBERS FOR SCANNING ELECTROCHEMICAL MICROSCOPY 16

2.1 ABSTRACT 16

2.2 INTRODUCTION 16

2.3 MODEL 17

2.4 EXPERIMENTAL 23
2.4.1 Chemicals and Reagents 23
2.4.2 Electrode Fabrication 23
2.4.3 Electrochemical Measurements 27
2.5 RESULTS AND DISCUSSION 27
2.5.1 Fabrication of Conical Probes based on Selectively Etched Optical Fibers and Characterization by SEM 27
2.5.2 Steady-state Cyclic Voltammetry 31
2.5.3 SECM Approach Curve Measurements 33
2.5.4 SECM Approach Measurements at Smaller Electrodes 36
2.5.5 Insulation with Electrophoretic Paint by Multiple Coating 36
2.5.6 Gold Quality of the Electrodes 41
2.6 CONCLUSIONS 41
2.7 REFERENCES 43
3.0 FABRICATION AND CHARACTERIZATION OF NANO-PROBES FOR SECM 44
3.1 ABSTRACT 44
3.2 INTRODUCTION 44
3.3 EXPERIMENTAL 48
3.3.1 FIB Milling of the Selectively Etched Optical Fibers 48
3.4 RESULTS AND DISCUSSION 48
3.4.1 Focused Ion Bean Modification of SECM Probes 48
3.4.2 Insulating the Gold-Coated Selectively Etched Optical Fibers with Sputtering of SiO_x 50
3.5 CONCLUSION 60
3.6 REFERENCES 61
APPENDIX A 62
APPENDIX B 64
4.0 FUTURE WORK 65
4.1 OPTIMIZATION OF SIOX COATING 65

4.2 OXYGEN TRANSFER AT WATER/FLUOROCARBON INTERFACE BY SECM 65
4.3 COMBINED SECM/OPTICAL MICROSCOPY 66
4.4 REFERENCES 66

LIST OF FIGURES

Figure 1.1 Probe chemical reactions across biological membranes 2
Figure 1.2 Principle of SECM. (A) positive feedback and (B) negative feedback. UME shown here is a cone electrode. 4
Figure 1.3 Approach curves as a function of the heterogeneous reaction rate constant for electron transfer at the substrate, k, $I_T=i_t/i_\infty$. From top to bottom, k (cm/s) is (a) 1, (b) 0.5, (c) 0.1, (d) 0.025, (e) 0.015, (f) 0.01, (g) 0.005, (h) 0.002, (i) 0.0001. Curve (a) is identical to that for mass transfer control and curve (i) for an insulating substrate[1]. 5
Figure 1.4 Theoretical SECM approach curves of tips at (a) a conductive and (b) an insulating substrate with different geometry. RG=10 for all electrodes[18, 19] except ring (RG=8).[20] 7
Figure1.5 RG effect on negative feedback in SECM (shown for a disk UME) 8
Figure 1.6 (a) Schematic top view of the ring microelectrode (b) SEM image[32] 12
Figure 2.1 Diagram of space domain for the numerical analysis of a conical electrode. The electrode geometry was determined from SEM..... 18
Figure 2.2 Concentration profile of the mediator near a conical probe approaching a conductor (d/a=1)..... 20
Figure 2.3 Concentration profile of the mediator near a conical probe approaching a insulator (d/a=1)..... 21
Figure 2.4 Modified geometry of the simulation space for numerical analysis of a conical electrode (a < 500 nm). 22
Figure 2.5 Schematic drawing of multistep index optical fibers. 24
Figure 2.6. Electrode profile 26
Figure 2.7 SEM image of selectively etched optical fibers after etching for 60min. 28
Figure 2.8 SEM image of selectively etched optical fibers after etching for 80min. 29
Figure 2.9 SEM image of a conical electrode after insulation..... 30

Figure 2.10 Cyclic votammogram from a conical probe in a aqueous solution of 1mM 1,1′-ferrocenedimethanol and 0.1 M KCl. Scan rate, 0.01 V/s. 32
Figure 2.11 Experimental SECM approach curve (solid line) at a Pt substrate as obtained with the conical microelectrode used for cyclic voltammetry in Fig. 2.10. Solution contained 1 mM 1, 1'-ferrocenedimethanol and 0.1 M KCl in water. The circles represent the theoretical curve for a conical electrode with the tip angle of 80° (See Fig. 2.1 for the insulating layer geometry). The dotted line represents an approach curve of a disk-shaped electrode, where the disk radius and the outer radius of the insulating layer are *a* and 2*a*, respectively..... 34
Figure 2.12 Experimental approach curves (solid lines) (a) over a polychlorotrifluoroethylene substrate at the same probe as used for Figs. 2.10 and 2.11 and (b) over a glass substrate at a conical electrode with the base radius of 0.70 μm. Solution contained 1 mM 1, 1'-ferrocenedimethanol and 0.1 M KCl in water. The circles represent the theoretical curve for a conical electrode with the tip angle of 80° (see Fig. 2.1 for the insulating layer geometry). The dotted lines represent an approach curve of a disk-shaped electrode, where the disk radius and the outer radius of the insulating layer are *a* and 2*a*, respectively..... 37
Figure 2.13 Comparison of theoretical (circles) and experimental SECM (solid line) curves at a Pt substrate for conical electrodes with base radius: (a) 255 nm and (b) 382 nm. The geometry for simulation is based on Fig. 2.4 with R=0.156a. The dashed line represents a theoretical approach curve of a disk-like electrode with RG=2. Triangles represent theoretical approach curve at a conical electrode with geometry defined in Fig. 2.1. Solution contained 1 mM 1,1′-ferrocenedimethanol and 0.1 M KCl in water. 38
Figure 2.14 Cyclic votammogram from probes prepared by repeated polymer applications in an aqueous solution of 1 mM 1,1′-ferrocenedimethanol and 0.1 KCl. Scan rate 0.01 V/s. 39
Figure 2.15 SEM images of a probe prepared by repeated polymer applications. 40
Figure 2.16 Electrode with bad gold coating. 42
Figure 3.1 Schematic of FIB milling after electrophoretic paint insulation 46
Figure 3.2 Schematic of FIB milling before electrophoretic paint insulation 47
Figure 3.3 Schematic of nanoelectrode fabrication by sputtering of silicon oxide and FIB 47
Figure 3.4 SEM images of a gold-coated probe modified by FIB..... 49
Figure 3.5 SEM images of a probe modified by FIB: (a) side view (b) top view. 51

Figure 3.6 Cyclic votammogram from the electrode in Fig. 3.4 in an aqueous solution of 1 mM 1,1′-ferrocenedimethanol and 0.1 M KCl. Scan rate 0.01 V/s. 52
Figure 3.7 Comparison of experimental SECM curve (solid line) and theoretical (black square) curve (ring electrode, RG=1.5) at a Pt substrate for probe in Fig. 3.4. Solution contains 1 mM 1,1′-ferrocenedimethanol and 0.1 M KCl. 53
Figure 3.8 SEM image of a gold-coated probe after sputtering of silicon oxide with RF diode at 250 W. 54
Figure 3.9 SEM image of a gold-coated probe after sputtering of silicon oxide with RF diode at: (a) 200 W and (b) 150 W 55
Figure 3.10 SEM image of a gold-coated probe after sputtering of silicon oxide with RF magnetron at 100 W. 56
Figure 3.11 Schematic of probe scan 57
Figure 3.12 Comparison for experimental probe scan curve (solid line) with theoretical one (cylindrical UME, dashed line). Solution contains 1 mM 1,1′-ferrocenedimethanol and 0.1 M KCl. 58
Figure 3.13 Evolution of the diffusion layer at an electrode with pinholes. (a) short time scale (b) long time scale. Dotted lines show surface of equal concentration in the diffusion layer. Arrows indicate concentration gradient driving the flux toward the electrode surface. 59

1.0 INTRODUCTION

1.1 FAST AND LOCAL CHEMICAL REACTIONS AT BIOLOGICAL MEMBRANES

Molecular transport through membranes is very important in life science. The reactions at the biological membranes are generally very fast and highly localized. It is well known that biomembrane surface is laterally highly heterogeneous in nanometer scale. To get insights of the transport process through nanometer-sized membrane structures (e.g., nuclear pore (~90 nm), lipid domains (100-500 nm), and neuronal vesicles (20-500 nm)), one needs to have a reliable methodology with comparable time and spatial resolution.

Scanning electrochemical microscopy (SECM) is a well-established technique and has several unique advantages in studying membrane transport processes:[1-6]

1) high spatial resolution defined by the probe size
2) capacity of measuring fast reactions
3) non-contact measurement
4) no externally applied potential applied across the membrane
5) selective detection of a mediator molecule

Development of nanometer-sized probes for SECM will allow us to take all of these advantages for studying molecular transports through the membrane nano-structures.

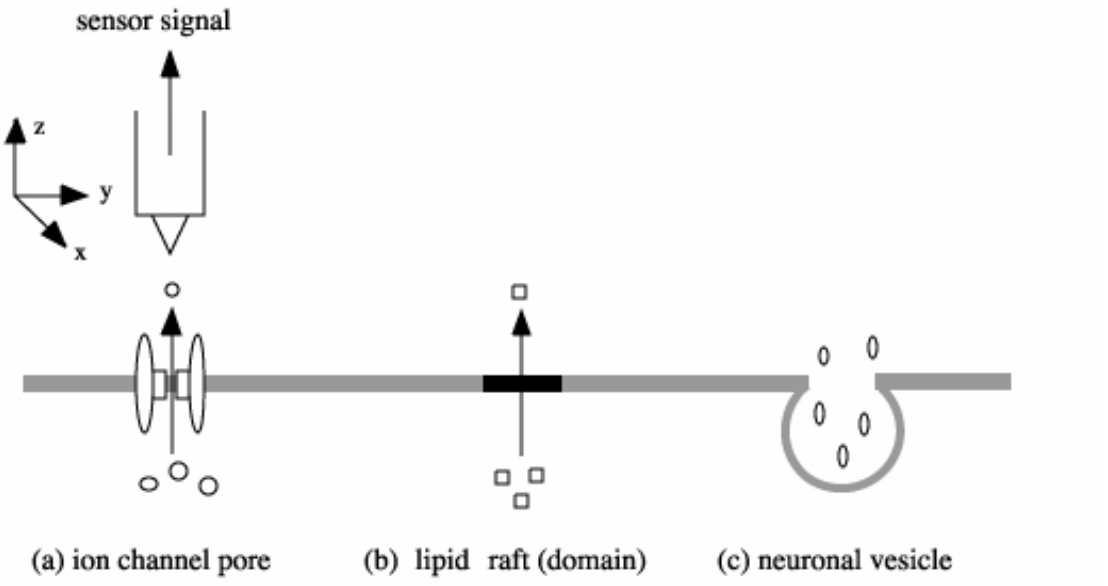

Figure 1.1 Probe chemical reactions across biological membranes

1.2 SCANNING ELECTROCHEMICAL MICROSCOPY (SECM)

SECM involves the measurement of the current through an ultramicroelectrode (UME) (an electrode with a radius, *a*, of the order of a few nm to 25 μm) when it is brought in close proximity of a substrate.[1] The materials for substrates can be either solids (e.g., glass, metal, polymer, biological material) or liquids (e.g., mercury, immiscible oil). The electrochemical response of the tip is perturbed by the substrate, which in turn will give the information of the reactivity and topography of the substrate. The tip can be moved normal to the surface (the z direction), or the tip can be scanned at constant z across the surface (the *x* and *y* directions).[7]

In order to understand the operation of SECM, one needs to understand the electrochemistry at small electrodes. It was not until 25 years ago that electrochemists began to appreciate the intriguing applications of UMEs in electroanalytical world.[8-10] Initially, they were attracted by the advantages of UME to overcome the limitations of conventional electrodes in the aspects of charging current and uncompensated resistance.[11] The rate of mass transport at very small electrodes is so high that kinetics measurements can be carried out by steady-state measurements rather than transient techniques.[12] By decreasing the size of a microelectrode from micrometer to

nanometer range, the study of the kinetics of very fast electrochemical and chemical reactions should be possible.[13] The electrode size is also critical for electrochemical imaging and is the main parameter determining the resolution in SECM.[14-16]

In the feedback mode of SECM, a UME is served as the working electrode and a redox mediator is either reduced or oxidized at the electrode tip so that a diffusion-limited steady-state current, i_{SS}, is obtained when the electrode is far from the substrate.

$$O + ne^- \rightarrow R \qquad (1)$$

where n is the stoichiometric number of electrons transferred in the tip reaction. The steady-state current for a microelectrode is given by:

$$i_{ss} = nFDcax \qquad (2)$$

where F is the Faraday constant, D is the diffusion coefficient of the redox mediator, c is the bulk concentration of the mediator, a is the tip radius and x is a constant depending on the electrode geometry.

As the tip approaches to a conductive substrate, the R species formed in reaction (1) diffuses to the substrate where it may be oxidized back to O:

$$R - ne^- \rightarrow O \qquad (3)$$

This process produces additional flux of O and hence increases the tip current, i_T ($i_T > i_{ss}$). This increase of current with distance is called positive feedback (Fig. 1.2A). In the limit as the distance d between tip and substrate approaches zero, the tip current will get very large where electron tunneling can occur.[1]

If the tip is brought to an insulated substrate, the tip-generated species, R, could not react on the inert substrate. At small d (i.e., within a few tip radii), $i_T < i_{ss}$ because the insulated substrate hinders the diffusion of species O to the tip from the bulk solution. Indeed, the smaller the tip-substrate separation, the smaller the tip current (negative feedback, Fig. 1.2B).

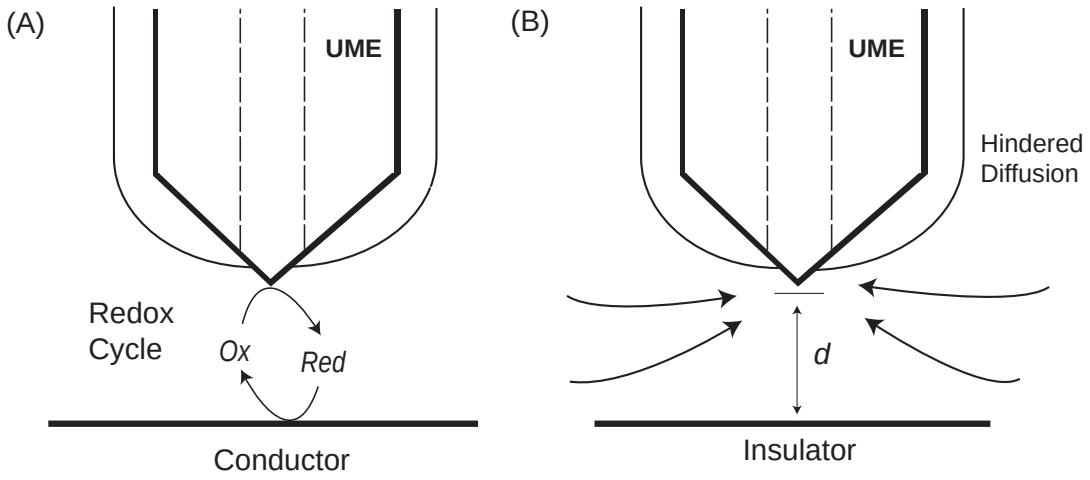

Figure 1.2 Principle of SECM. (A) positive feedback and (B) negative feedback. UME shown here is a cone electrode.

By recording an approach curve with the tip close to a substrate, one can study the rates of electron transfer at the surface of the substrate. Because mass transfer rates at the small electrodes are high, measurements of fast reactions without interference of mass transfer are possible.[1] Fig 1.3 illustrates approach curves (normalized tip current vs. normalized distance) as a function of the heterogeneous reaction rate constant for electron transfer at the substrate. It indicates that by comparing the approach curves we can obtain information of the surface reactivity.

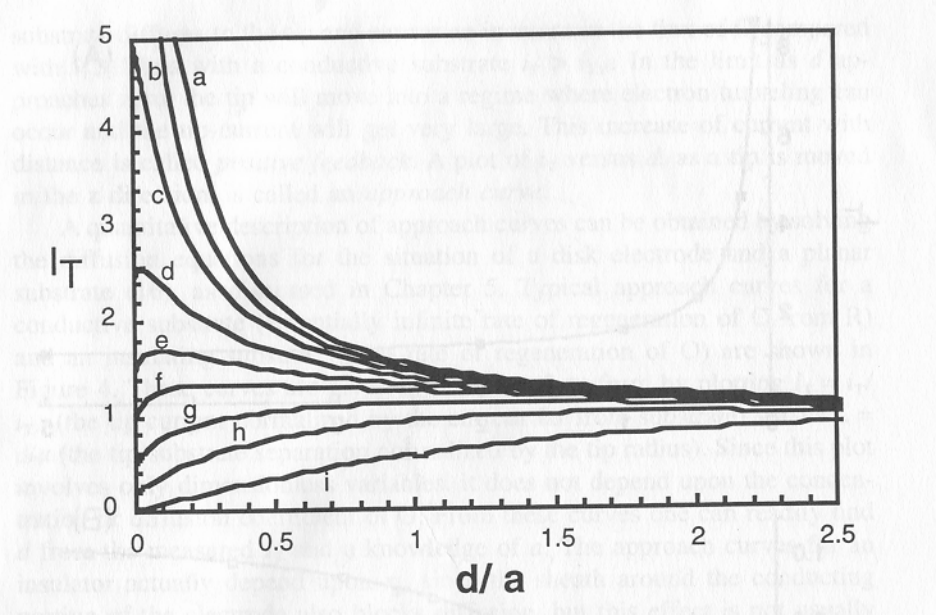

Figure 1.3 Approach curves as a function of the heterogeneous reaction rate constant for electron transfer at the substrate, k, $I_T=i_t/i_\infty$. From top to bottom, k (cm/s) is (a) 1, (b) 0.5, (c) 0.1, (d) 0.025, (e) 0.015, (f) 0.01, (g) 0.005, (h) 0.002, (i) 0.0001. Curve (a) is identical to that for mass transfer control and curve (i) for an insulating substrate[1].

1.3 EFFECT OF TIP GEOMETRY

To accurately measure the reactivity or the topography of a substrate surface, one needs to have a well-defined probe for SECM, because the tip current is also affected by the tip shape and the tip-substrate separation. Therefore, a slight change in tip geometry will affect the outcome of the tip current in SECM.

In voltammetric analysis, the geometry of ultramicroelectrodes does not need to be precisely controlled because electrodes with different geometry have similar voltammograms.[17]

On the other hand, electrodes with different geometry show totally different behaviors when they approach very close to the surface of a conductive or an insulating substrate in SECM (Fig. 1.4). This result indicates that SECM can be used to determine a probe's geometry and size. And at the same time, electrode with well-defined geometry is necessary for quantitative SECM experiments, which is highly challenging at nanometer scale.

Fig. 1.4 demonstrates the effect of different tip geometry on the shape of SECM approach curves, meanwhile, RG (RG= diameter with insulating sheath/ diameter of the metal core) values also affect the SECM curves, especially for negative feedbacks. With insulating substrates, a smaller RG value results in a higher current at any distance between tip and substrate, since the contribution of back diffusion (diffusion from behind the insulating sheath) is not negligible when the thickness of the insulating layer becomes thinner (Fig. 1.5).

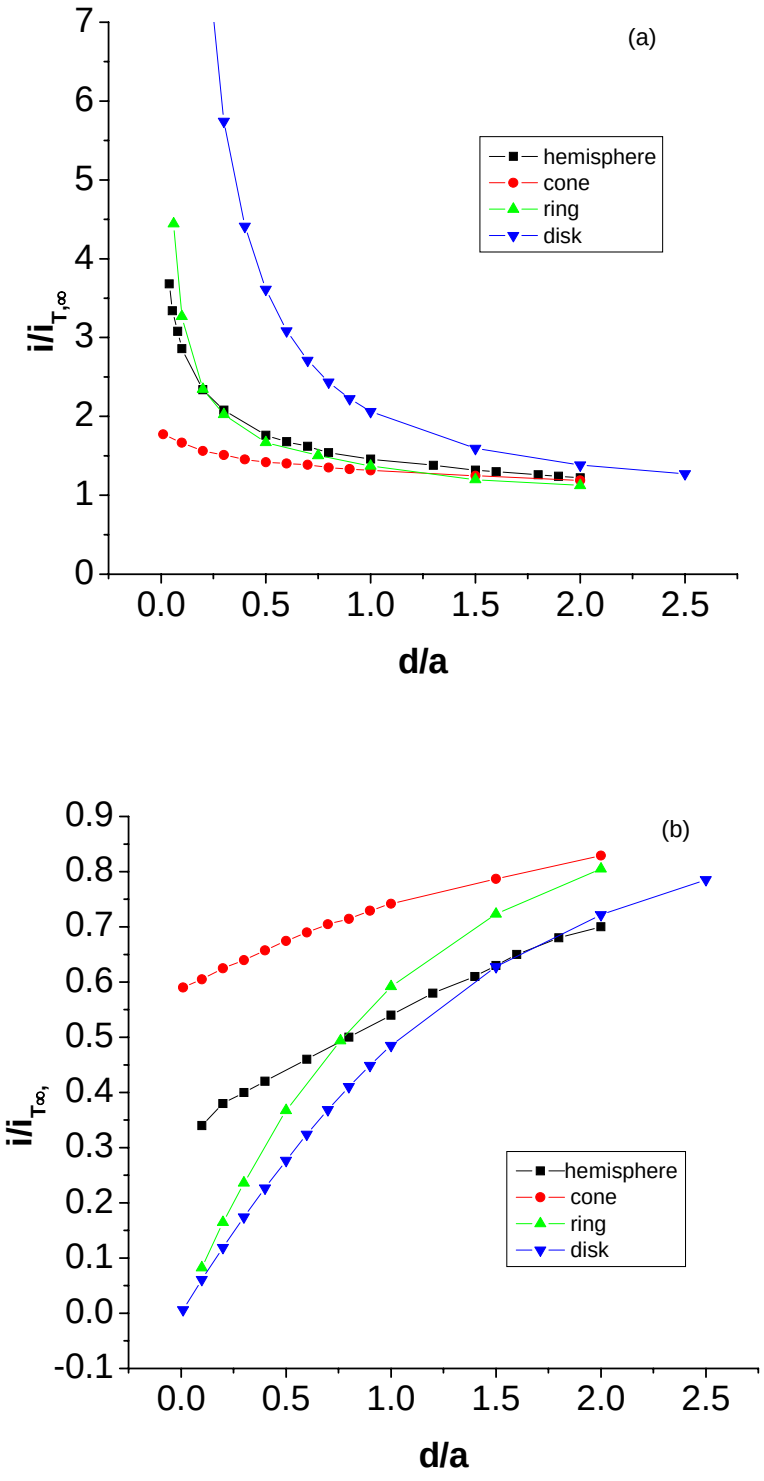

Figure 1.4 Theoretical SECM approach curves of tips at (a) a conductive and (b) an insulating substrate with different geometry. RG=10 for all electrodes[18, 19] except ring (RG=8).[20]

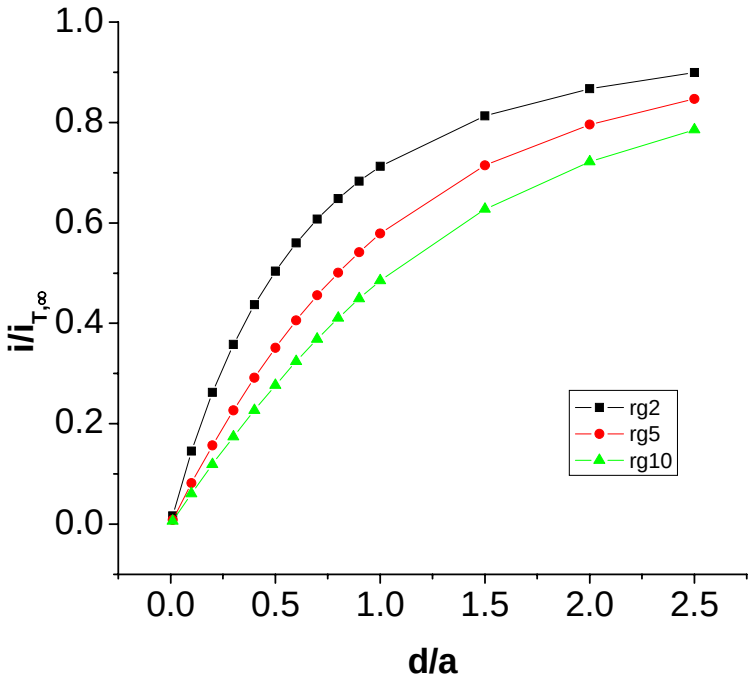

Figure1.5 RG effect on negative feedback in SECM (shown for a disk UME)

1.4 FABRICATIONS OF PROBES FOR SECM

The information, which could be obtained by SECM, depends strongly on the shape and size of the tip. As the advantages of SECM measurements, fast mass transport and high spatial resolution, arise from the small tip size, the development of reliable techniques for the fabrication of nanometer-sized electrode with well-defined geometry was sought by many research groups.

1.4.1 Disk-in-glass Microelectrode

Early experiments in SECM employed metal (or carbon) disk electrodes.[7, 9]This kind of disk-in-glass electrodes were prepared by sealing a micrometer-sized fine metal wire in glass and

polishing the sealed end with sandpaper until the cross section of the wire is exposed and then with alumina paste. Electrical connection to the unsealed end of the wire is made by Ag epoxy to a copper wire. The tip of the electrode was sharpened manually so that a small RG could be obtained, which will decrease the possibility of the contact between the glass wall and the substrate because of any slight tilt in the axial alignment of the tip as the tip approaches the substrate. This technique has been successfully used to prepare tips of diameter larger than 1 μm (2 μm disk electrode is commercially available). Preparation of submicron SECM tips by this method is very challenging.

Reduction of the size of SECM probes is important, since the resolution of SECM depends strongly on the size of tip used. In order to achieve this goal, one has to decrease the diameter of commercially available metal wires by electrochemically etching or by pulling in glass capillary as described below. Further coating and exposing steps, are needed for the etched wires, to expose only the electrode surface.

1.4.2 Submicrometer Glass-Encapsulated Microelectrodes

An alternative way to prepare submicron glass-encapsulated SECM tips is done by pulling metal wires with the glass capillary using a laser pipette puller.[21-23] Platinum or silver microwires (50-μm diameter) and borosilicate tubes (1.2 mm outer diameter) were used as starting materials. The parameters for the pulling program could be varied in order to control the size and shape of the micropipette. Right after pulling, the metal core is completely covered with glass and further step is needed to expose the tip of the wire. This was done by micropublishing. The size of the prepared tip increases with the polishing time. Small planar tips made by this method with effective radii from 20 to 500 nm exhibited well-behaved voltammetry. However, only for relatively large tips (a $>$ 100 nm), the results from voltammetric, SEM and SECM characterizations would agree with each other, which is the premise for quantitative electrochemical measurements. Moreover, the RGs of the electrodes made by this method were usually quite large, which prevents bringing the electrode very close to the substrate as the insulating wall might strike the substrate surface.

1.4.3 Electrochemical Etching of Metal Wires and Insulation by Electrophoretic Paint

Electrochemical etching of metal microwires, based on anodic dissolution of the end of the wire, gives the very end of the wire a tapered shape. Further insulation of the wire and exposition of only the very end of the tip is needed to manufacture small tips.

There are two ways to etch the wire electrochemically[1]: an alternating current (ac) etch or direct etch (dc) according to the applied potential. The outcome of the tip shape varies with different etching procedure: the ac-etched tips have a conical shape and much larger cone angles than the dc etched tips. The dc-etched tips, on the other hand, have the shape of a hyperboloid and are much sharper than ac-etched tips.[1] To insulate the etched metal wire and expose the tip, the conventional way is to use anodic electrophoretic paint introduced by Schulte and co-workers.[24-26] The electrodes made from etched metal wires usually can achieve nanometer size, however, the geometry of such electrodes is not well-defined.[27, 28]

1.4.4 Self-assembled Spherical Gold UME

Fabrication of self-assembled spherical gold UME was developed by Bard and co-workers[29], based on the finding by Schiffrin and co-workers, who found that nanometer-sized Au particles can be self-assembled to electronically conductive bulk materials[30] and multilayer thin films,[30] by the use of dithiol cross-linking agents. The fabrication technique involves confining the dithiol linker inside the micrometer-sized tip of a pulled capillary that was then immersed into a solution of Au particles. Well-developed spheres with a golden metallic luster grow at the end of the tip. If a conductive carbon coating is applied prior to the preparation of the self-assembled electrode, the microspheres can be electrically contacted. The size of the spherical electrodes could be controlled by the dithiol concentration or by the size of the pulled capillary. However, the spherical shape of the electrode causes less feedback effect in SECM.

1.4.5 Ring Microelectrode by Focuses Ion Beam (FIB)

The fabrication of a ring microelectrode in an AFM tip with FIB has been reported by Kranz and co-workers.[31, 32] They used FIB to sculpture a ring shape on a gold-coated and Si_3N_4-insulated AFM tip (Fig. 1.6). FIB milling is a modern technique in designing and sculpturing nano- and micro-meter structures with high precision. This technique was mainly developed during the late 1970s and the early 1980s, and the first commercial instruments were introduced more than a decade ago.[33] The key ability of FIB technology is its capability to localize the modification to only the area requiring alternation. The results from Kranz et al. showed that FIB is well suited for modifying the geometry of the electrode, however, the insulating protruded part on their tip prevents it from approaching a substrate very closely for SECM application.

1.5 DESIGN AND CONSTRUCTION OF SUB-MICROMETER PROBES FOR SECM

The UMEs fabricated for SECM are so far mostly restricted to the micrometer range. Submicrometer-sized SECM probes are required for characterization of localized microenvironment such as nuclear transports through the nuclear pore complex with high spatial resolution. The fabrication and even more the characterization of submicrometer-sized electrodes have proved to be difficult. For an electrode to be used as a SECM probe, its geometry must be perfectly known especially if any meaningful quantitative measurements are to be made with it.[13, 18, 34-37] The development of techniques aimed at fabricating submicrometer-sized electrodes of highly characterized geometry and suitable as tips for SECM is therefore very desirable.

The aim of present work was to construct SECM probes of submicrometer dimension with well-defined geometry.

1.5.1 Selectively Etched Optical Fibers

Optical fibers were first employed as microelectrodes for simultaneous electrochemical measurements in the early 90s.[38, 39] Since then, they become more important as the templates for

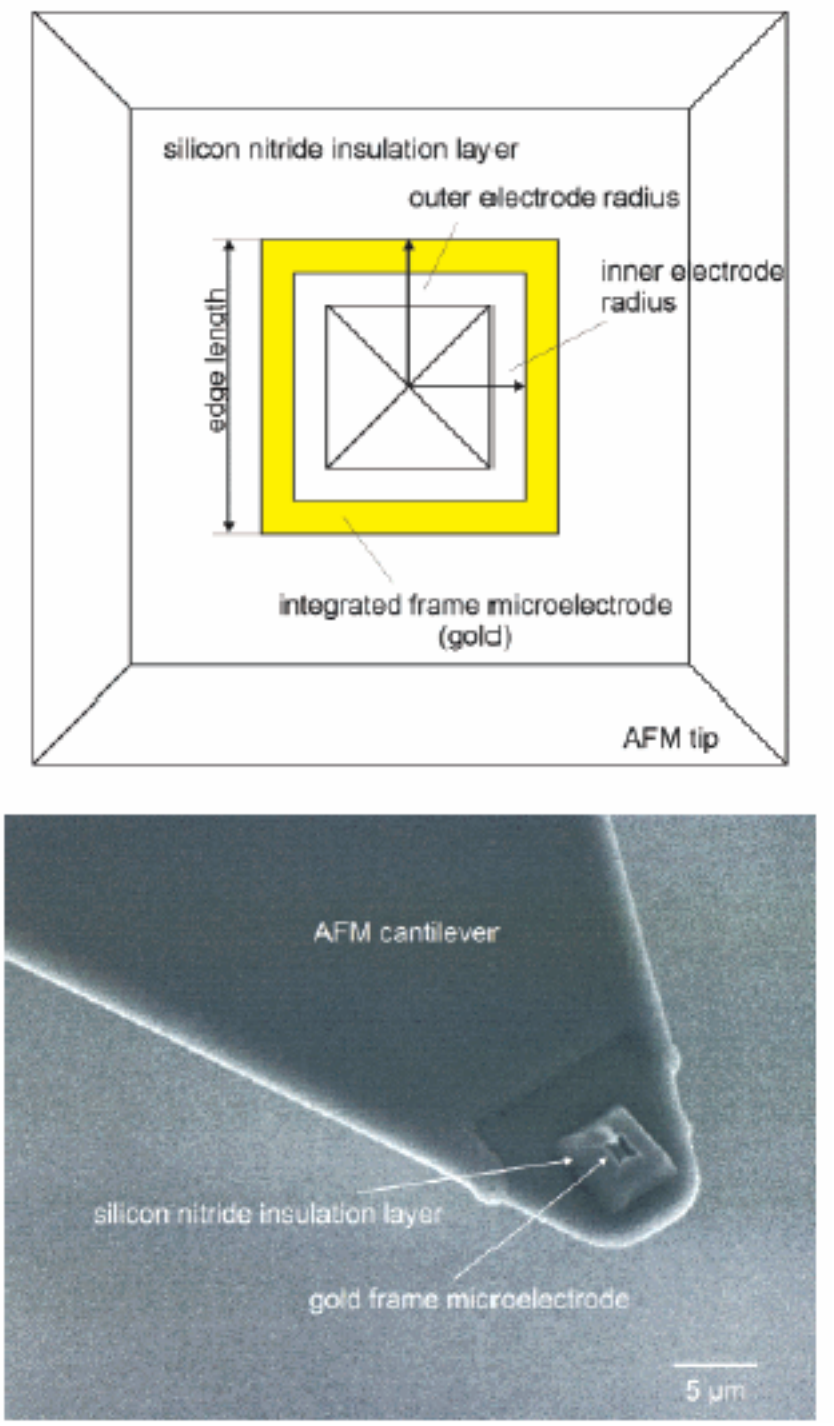

Figure 1.6 (a) Schematic top view of the ring microelectrode (b) SEM image[32]

the fabrication of probes for scanning photoelectrochemical microscopy[40, 41] and scanning electrochemical/optical microscopy,[42, 43] which allow the simultaneous measurements at microenvironments. The conventional way to fabricate such probes based on optical fibers is: (1) heating and pulling of optical fiber (2) metal coating (3) electrical insulation and (4) tip exposure. This method is typical in fabrication of near-field scanning optical microscope (NSOM) probes.[44] However, the electrodes made by the first step are not reproducible and the sharpness of the fibers is limited down to ~50nm in diameter.

In our work, we propose[45] a selective etching technique to reproducibly fabricate probes with defined geometry. High-GeO_2-doped optical fibers are chemically etched to a sharp point (10 nm in diameter)[46] in NH_4F/HF buffer solutions, due to the difference of the etching rate in high-GeO_2-doped fiber core and cladding layers. Also, we can easily adjust the apex angle of the fiber electrode by simply varying NH_4F/HF ratio and etching time.

1.5.2 Electrophoretic Paint Technique

Bard and co-workers successfully fabricated the smallest electrochemical/optical probe through electrophoretic paint, which can be used for simultaneous "far-field" optical/electrochemical imaging.[42] Their results indicated that this technique is very reproducible and easy to control, which is much better than other insulating techniques. Therefore, we thought it's a suitable technique for insulating our selectively etched optical fibers reproducibly. With this technique, we successfully fabricated well-defined conical sub-micrometer probes for SECM.

1.5.3 FIB Milling

Because FIB enables localized milling with nanometer precision, we thought it would be a good attempt to apply FIB in modifying our selectively etched fiber probes.

1.6 REFERENCES

(1) Bard, A. J.; Mirkin, M. V.; *Scanning Electrochemical Microscopy*, 2001.

(2) Tsionsky, M.; Zhou, J. F.; Amemiya, S.; Fan, F. R. F.; Bard, A. J.; Dryfe, R. A. W. *Analytical Chemistry* **1999**, *71*, 4300-4305.

(3) Amemiya, S.; Bard, A. J. *Analytical Chemistry* **2000**, *72*, 4940-4948.

(4) Yamada, H.; Matsue, T.; Uchida, I. *Biochem. Biophys. Res. Commun.* **1991**, *180*, 1330-1334.

(5) Barker, A. L.; Macpherson, J. V.; Slevin, C. J.; Unwin, P. R. *J.Phys.Chem.B* **1998**, *102*, 1586-1598.

(6) Barker, A. L.; Unwin, P. R. *J.Phys.Chem.B* **2001**, *105*, 12019-12031.

(7) Bard, A. J.; Fan, F. R. F.; Kwak, J.; Lev, O. *Analytical Chemistry* **1989**, *61*, 132-138.

(8) Ponchon, J.-L.; Cespuglio, R.; Gonon, F.; Jouvet, M.; Pujol, J.-F. *Analytical Chemistry* **1979**, *51*, 1483-1486.

(9) Dayton, M. A.; Brown, J. C.; Stutts, K. J.; Wightman, R. M. *Analytical Chemistry* **1980**, *52*, 946-950.

(10) Wightman, R. M. *Analytical Chemistry* **1981**, *53*, 1125A.

(11) Mirkin, M. V.; Horrocks, B. R. *Analytica Chimica Acta* **2000**, *406*, 119-146.

(12) Bond, A. M.; Oldham, K. B.; Zoski, C. G. *Journal of Electroanalytical Chemistry* **1989**, *216*, 177.

(13) Mirkin, M. V.; Fan, F. R. F.; Bard, A. J. *Journal of Electroanalytical Chemistry* **1992**, *328*, 47-62.

(14) Kwak, J.; Bard, A. J. *Analytical Chemistry* **1989**, *61*, 1794-1799.

(15) Lee, C.; Miller, C. J.; Bard, A. J. *Analytical Chemistry* **1991**, *63*, 78-83.

(16) Bard, A. J.; Mirkin, M. V.; Unwin, P. R.; Wipf, D. O. *Journal of Physical Chemistry* **1992**, *96*, 1861-1868.

(17) Oldham, K. B.; Zoski, C. G. *J. Electroanal. Chem.* **1988**, *256*, 11-19.

(18) Fulian, Q.; Fisher, A. C.; Denuault, G. *Journal of Physical Chemistry B* **1999**, *103*, 4387-4392.

(19) Zoski, C. G.; Liu, B.; Bard, A. J. *Analytical Chemistry* **2004**, *76*, 3646-3654.

(20) Lee, Y.; Amemiya, S.; Bard, A. J. *Analytical Chemistry* **2001**, *73*, 2261-2267.

(21) Pendley, B. D.; Abruna, H. D. *Analytical Chemistry* **1990**, *62*, 782-784.

(22) Shao, Y. H.; Mirkin, M. V.; Fish, G.; Kokotov, S.; Palanker, D.; Lewis, A. *Analytical Chemistry* **1997**, *69*, 1627-1634.

(23) Fish, G.; Bouevitch, O.; Kokotov, S.; Lieberman, K.; Palanker, D.; Turovets, I.; Aaron, L. *Review of Scientific Instruments* **1995**, *66*, 3300-3306.

(24) Bach, C. E.; Nichols, R. J.; Beckmann, W.; Meyer, H.; Schulte, A.; Besenhard, J. O.; Jannakoudakis, P. D. *Journal of the Electrochemical Society* **1993**, *140*, 1281-1284.

(25) Schulte, A.; Chow, R. H. *Analytical Chemistry* **1996**, *68*, 3054-3058.

(26) Schulte, A.; Chow, R. H. *Analytical Chemistry* **1998**, *70*, 985-990.

(27) Slevin, C. J.; Gray, N. J.; Macpherson, J. V.; Webb, M. A.; Unwin, P. R. *Electrochemistry Communications* **1999**, *1*, 282-288.

(28) Watkins, J. J.; Chen, J. Y.; White, H. S.; Abruna, H. D.; Maisonhaute, E.; Amatore, C. *Analytical Chemistry* **2003**, *75*, 3962-3971.

(29) Demaille, C.; Brust, M.; Tsionsky, M.; Bard, A. J. *Analytical Chemistry* **1997**, *69*, 2323-2328.

(30) Brust, M.; Bethell, D.; Schiffrin, D. J.; Kiely, C. J. *Advanced Materials* **1995**, *7*, 795.

(31) Lugstein, A.; Bertagnolli, E.; Kranz, C.; Mizaikoff, B. *Surface and Interface Analysis* **2002**, 146-150.

(32) Kranz, C.; Friedbacher, G.; Mizaikoff, B.; Lugstein, A.; Smoliner, J.; Bertagnolli, E. *Analytical Chemistry* **2001**, *73*, 2491-2500.

(33) Melngailis, J. *Journal of Vacuum Science & Technology, B: Microelectronics and Nanometer Structures* **1987**, *5*, 469-495.

(34) Baranski, A. S. *J. Electroanal. Chem.* **1991**, *307*, 287-292.

(35) Abbou, J.; Demaille, C.; Druet, M.; Moiroux, J. *Analytical Chemistry* **2002**, *74*, 6355-6363.

(36) Oldham, K. B. *Analytical Chemistry* **1992**, *64*, 646-651.

(37) Fulian, Q.; Fisher, A. C.; Denuault, G. *Journal of Physical Chemistry B* **1999**, *103*, 4393-4398.

(38) Pennarun, G.; Boxall, C.; O'Hare, D. *Analyst (Cambridge, United Kingdom)* **1996**, *121*, 1779-1788.

(39) Kuhn, L. S.; Weber, A.; Weber, S. G. *Analytical chemistry* **1990**, *62*, 1631-1636.

(40) Casillas, N.; James, P.; Smyrl, W. H. *Journal of the Electrochemical Society* **1995**, *142*, L16-L18.

(41) James, P.; Casillas, N.; Smyrl, W. H. *Proceedings - Electrochemical Society* **1996**, *95-15*, 425-434.

(42) Lee, Y.; Bard, A. J. *Analytical Chemistry* **2002**, *74*, 3626-3633.

(43) Lee, Y.; Ding, Z. F.; Bard, A. J. *Analytical Chemistry* **2002**, *74*, 3634-3643.

(44) Betzig, E.; Trautman, J. K. *Science* **1992**, *257*, 189-195.

(45) Xiong, H.; Guo, J.; Kurihara, K.; Amemiya, S. *Electrochemistry Communications* **2004**, *6*, 615-620.

(46) Ohtsu, M.; Editor *Near-Field Nano/Atom Optics and Technology*, 1998.

2.0 FABRICATION AND CHARACTERIZATION OF CONICAL MICROELECTRODE PROBES TEMPLATED BY SELECTIVELY ETCHED OPTICAL FIBERS FOR SCANNING ELECTROCHEMICAL MICROSCOPY

2.1 ABSTRACT

Selectively etched optical fibers were used as a template for fabrication of ultramicroelectrodes (UME), which are suitable for use as a probe in scanning electrochemical microscopy (SECM). Multistep index optical fibers with high-GeO_2-doped core and two cladding layers were chemically etched to a sharp point (10 nm in diameter) in NH_4F/HF buffer solutions. The etched fibers had a defined geometry and the etching process was highly reproducible. After etching, a layer of gold was sputtered on the fibers. The Au-coated fibers were then insulated by electrophoretic paint. The size and shape of the electrodes were determined by steady-state cyclic voltammetry and SECM. The SECM tip current-distance (approach) curves over conductive and insulating substrates agreed with the theoretical curves obtained by numerical simulations, which proves a conical electrode geometry. The base radius and height of the conical electrodes determined by SECM were in the range of 0.255-1.0 and 0.3-1.2 μm, respectively.

2.2 INTRODUCTION

Optical fibers were first employed as microelectrodes for simultaneous electrochemical measurements in the early 90s.[1, 2] Since then, they become more important as the templates for the fabrication of probes for scanning photoelectrochemical microscopy[3, 4] and scanning electrochemical/optical microscopy,[5, 6] which allow the simultaneous measurements at

microenvironments. The conventional way to fabricate such probes based on optical fibers is: (1) heating and pulling of optical fiber (2) metal coating (3) electrical insulation and (4) tip exposure. This method is typical in fabrication of near-field scanning optical microscope (NSOM) probes.[7] However, the electrodes made by the first step are not reproducible and the sharpness of the fibers is limited down to ~50nm in diameter.

In our work, we propose[8] a selective etching technique to reproducibly fabricate probes with defined geometry. High-GeO_2-doped optical fibers are chemically etched to a sharp point (10 nm in diameter)[9] in NH_4F/HF buffer solutions, due to the difference of the etching rate in high-GeO_2-doped fiber core and cladding layers. Also, we can easily adjust the apex angle of the fiber electrode by simply varying NH_4F/HF ratio and etching time. By coating etched fibers with a thin layer of Au through sputtering and then with an insulating polymer layer by electrophoretic paint technique, we successfully prepared conical electrodes in micro to sub-micrometer size. The probes were characterized by steady-state cyclic voltammetry, SECM and scanning electron microscopy (SEM).

2.3 MODEL

Theoretical SECM approach curves with conical probes have been obtained by analytical approximations[10] and later using numerical simulations based on the boundary element method[11]. There are also reports about steady-state limiting currents at finite conical microelectrodes[12]. However, none of them treated the geometry of the conical probes constructed here. Therefore, numerical simulations were carried out to describe the steady-state current at the conical tips as a function of the tip-substrate distance.

The geometry of the electrode is shown in Fig. 2.1, where the angles at the tip and the insulating layer were determined to be 80^o and 58^o, respectively, by SEM. The tip angle corresponds to the aspect ratio, *h/a*, of 1.2, where *a* is the base radius of the conical tip and *h* is the height.

Consider a one-step reaction

$$O + ne^- \Leftrightarrow R \qquad (1)$$

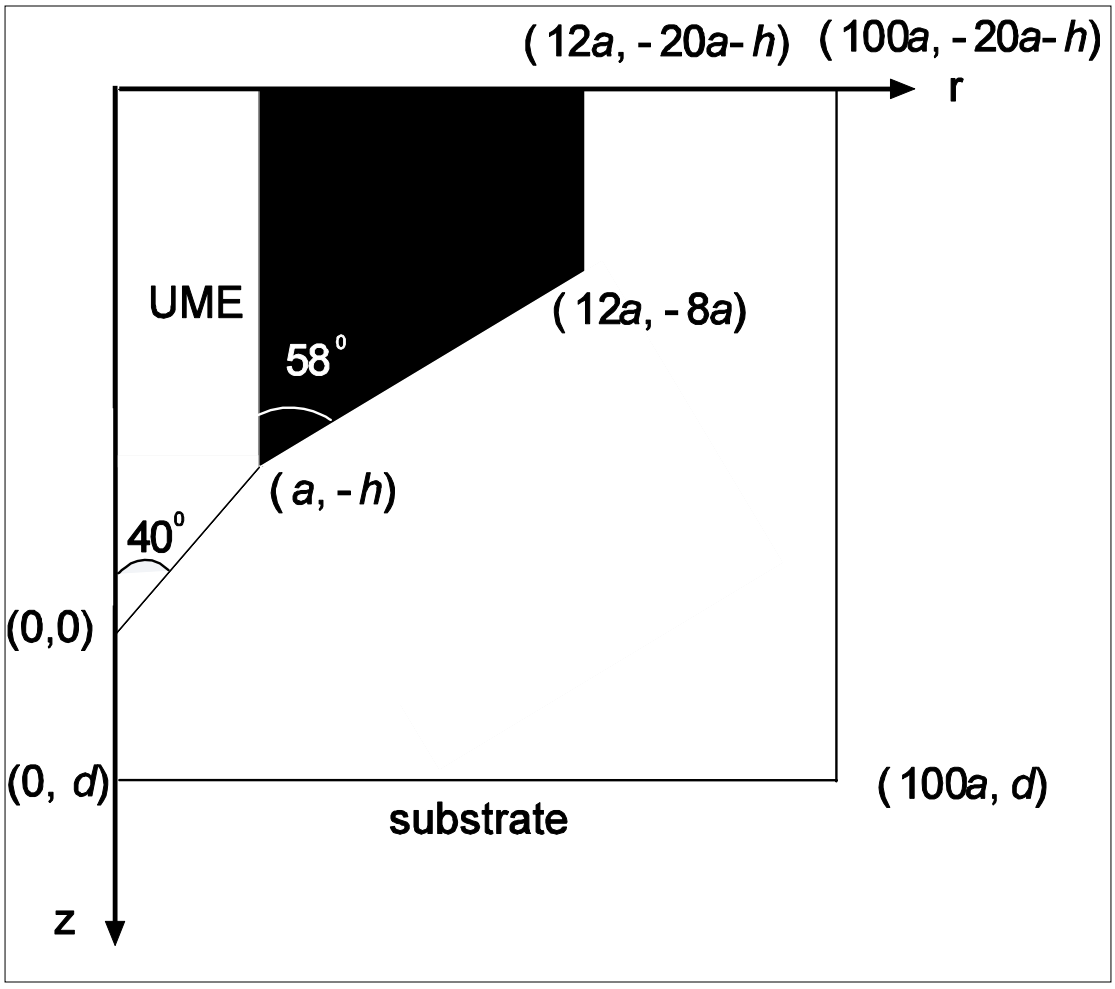

Figure 2.1 Diagram of space domain for the numerical analysis of a conical electrode. The electrode geometry was determined from SEM**.**

taking place at a conical electrode surface where species R reaches and species O leaves the electrode solely by diffusion. The steady-state diffusion equation in cylindrical coordination is

$$\frac{\partial c}{\partial t} = D(\frac{\partial^2 c}{\partial r^2} + \frac{1}{r}\frac{\partial c}{\partial r} + \frac{\partial^2 c}{\partial z^2}) = 0, \qquad (2)$$

where r and z are the coordinates in directions parallel and normal to the electrode base plane, respectively, c is the mediator concentration at (r, z), and D is the diffusion coefficient of the mediator. The boundary conditions are:

at conical electrode surface

$$c(r, -\frac{hr}{a}) = 0, \ 0 < r < a \qquad (3)$$

at insulation regions

$$[\frac{\partial c(r,z)}{\partial r}]_{r=12a} = 0, \ -20a\text{-}h < z < -8a, \qquad (4)$$

$$[\frac{\partial c(r,z)}{\partial N}] = 0, \ a < r < 12a, \qquad (5)$$

where $\partial c(r, z)/\partial N$ is the normal derivative of the mediator concentration at the peripheral insulating surface of the conical tip simulation space limit

$$c\ (r, z) = c_o, \ 12a < r < 100a, \ z = -20a\text{-}h, \qquad (6)$$

$$\text{and } r = 100a, \ -20a\text{-}h < z < d \qquad (7)$$

where c_o is the initial mediator concentration in the bulk solution and d is the tip-substrate distance.

axis of symmetry

$$[\frac{\partial c(r,z)}{\partial r}]_{r=0} = 0, \ 0 < z < d, \qquad (8)$$

$$[\frac{\partial c(r,z)}{\partial z}]_{z=d} = 0, \ 0 < r < 100a \text{ (insulating substrate)} \qquad (9)$$

$$c(r, d) = c_o, \ 0 < r < 100a \text{ (conductive substrate)} \qquad (10)$$

The steady-state current to the conical electrode, i, is given by integrating the flux over the electrode surface

$$i = 2\pi mFD\int_0^a r[\frac{\partial c(r,-\frac{hr}{a})}{\partial N}]dr, \qquad (11)$$

where $\partial c(r, -hr/a)/\partial N$ is the normal derivative of the mediator concentration at the electrode surface. The numerical solution of this SECM diffusion was solved with the program FEMLAB version 2.3 (COMSOL, Inc., Burlington, MA, USA), which uses the finite element method. The typical concentration profiles of the mediator near the probe at a conductive and an insulating substrate are shown in Fig. 2.2 and Fig. 2.3, respectively.

Simulations were further modified for smaller tips (a < 500 nm) as the tip sharpness becomes comparable to the tip size. The geometry of the probe was revised as shown in Fig. 2.4. And a parameter R (radius of inscribed circle) was introduced.

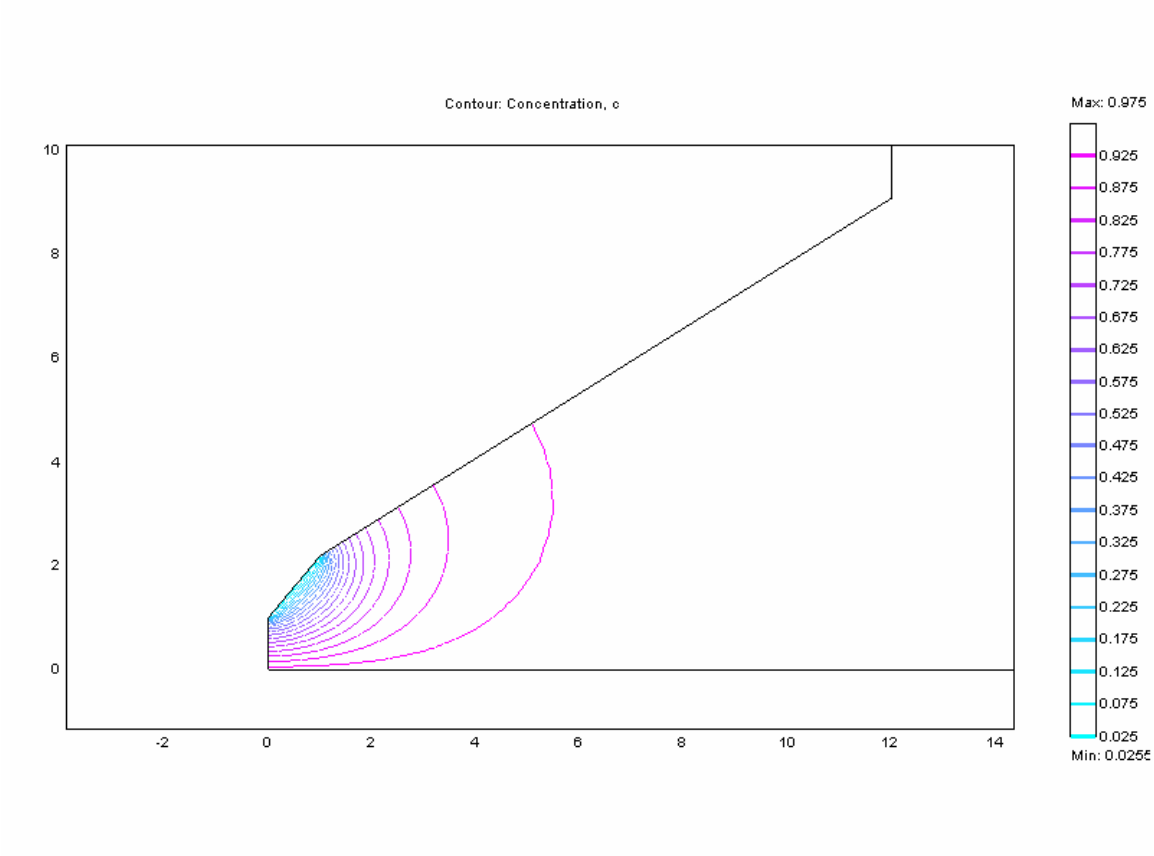

Figure 2.2 Concentration profile of the mediator near a conical probe approaching a conductor (d/a=1)

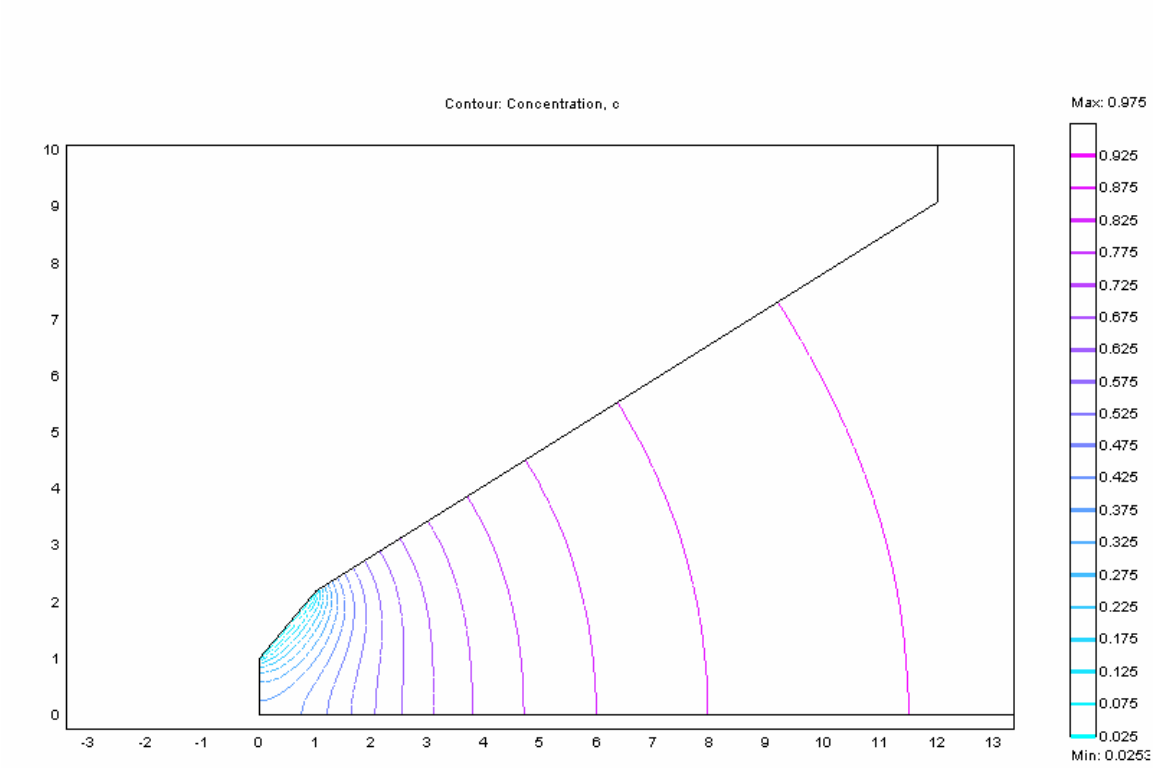

Figure 2.3 Concentration profile of the mediator near a conical probe approaching a insulator (d/a=1)

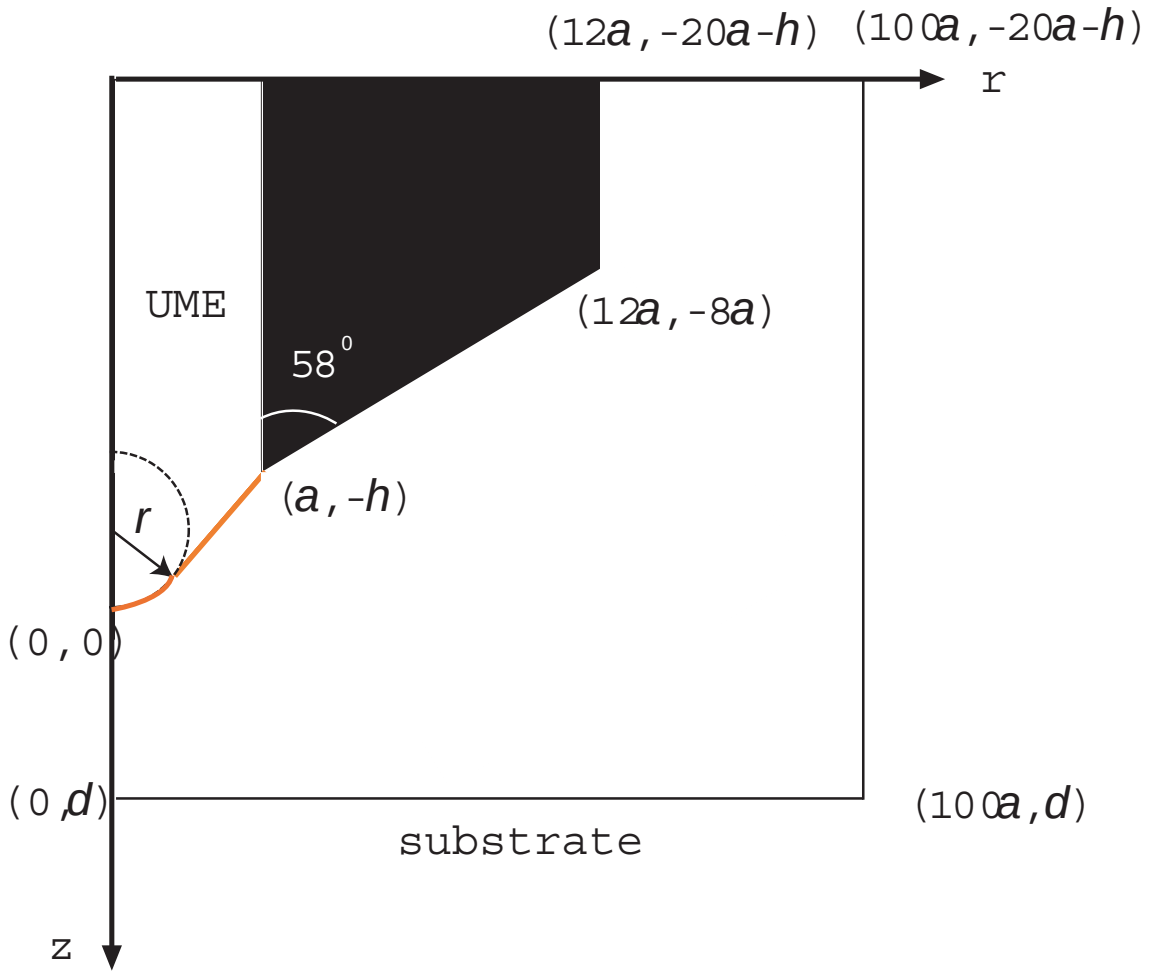

Figure 2.4 Modified geometry of the simulation space for numerical analysis of a conical electrode (a < 500 nm).

2.4 EXPERIMENTAL

2.4.1 Chemicals and Reagents

1,1′-ferrocenedimethanol (Sigma-Aldrich, St. Louis, MO, USA), KCl (J.T.Baker Chemical Co, Phillipsburgh, NJ, USA), sulfuric acid (J. T. Baker), NH_4F (Sigma-Aldrich) and HF (J.T. Baker) were reagent grade and used without further purification. All solutions were prepared with 18 $M\Omega\ cm^{-1}$ deionized water (Nanopure, Barnstead, Dubuque, IA, USA)

2.4.2 Electrode Fabrication

Multistep index optical fibers with GeO_2-doped SiO_2 core, SiO_2 inner cladding, and F-doped SiO_2 outer cladding (Fig.2.5) were obtained from Hoden Seimitsu Kako Kenkyusho, Kanagawa, Japan.[13] Optical fiber tips were prepared by stripping 1.5 cm of the insulating jacket from the tip of a 5-cm-long fiber with jacket remover JR-22 (Sumitomo, Electric Lightwave Copr., Research Triangle Park, NC, USA). The exposed portion of the fiber was cleaned with ethanol to remove any residual. A flat, smooth tip surface was obtained by cutting the exposed end of the fiber with fiber cleaver CT-20-12 (AFL Telecommunications, Franklin, TN, USA).

The fibers with smooth surfaces at the tips were then immersed in a NH_4F/HF etching solution. In order to optimize the solution composition as well as the etching time, the fiber tip was brought under an optical microscope BX-41 (Olympus America Inc., Melville, NY, USA) for investigation. Field-emission SEM equipped with an energy-dispersed analysis of X-rays (EDX) system, model XL-30 (Philips Electron Optics, Eindhoven, the Netherlands), was used to further determine the tip size and geometry. The optimum etching solution, which yields defined cone shape, consists of 40 wt% NH_4F, 48.0-51.0 wt% HF and water with volume ratio of 1.45:1:1.

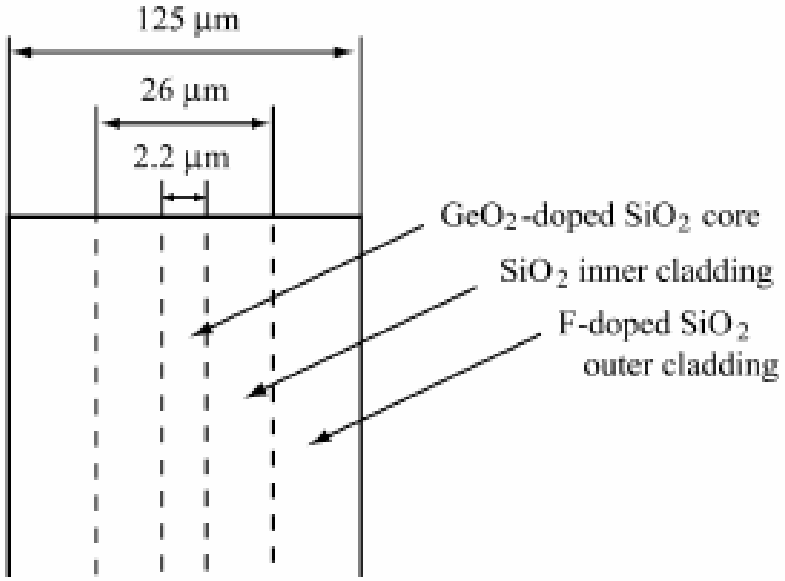

Figure 2.5 Schematic drawing of multistep index optical fibers.

An etched optical fiber was coated with a gold layer by sputter coater 108 auto (Ted Pella Inc., Redding, CA, USA). The fiber was vertically attached to a home-made stage so that the tapered tip is positioned toward the target. The tip-target distance was kept at 10 cm for reproducible coating. A flat glass substrate was simultaneously coated on the stage and the gold layer thickness on the glass was measured to be ~ 100 nm by atomic force microscope (DI 3100, Digital Instruments, Santa Barbara, CA, USA). Silver epoxy H20E (Epoxy Technology Inc., Billerica,MA, USA) was used to establish electrical connection via a Chrome wire.

The gold-coated fiber was immersed in a 1 M H_2SO_4 solution and scanned for 20 cycles at 1.5 V to clean the Au surface and thoroughly rinsed with deionized water. The insulation of the Au-coated fibers was carried out by electrophoretic paint method[5, 14, 15] originally developed by Bach et al. for coating STM tips[16, 17] and adapted by Schulte[18] for preparing carbon fiber microelectrodes. Slevin et al. used this method to prepare nanometer-scale Pt electrodes and electrochemical AFM tips,[14] which has then been adopted and modified by White's group[15] and Bard's group.[5] The gold-coated etched fiber was dipped in an aqueous anodic paint solution AE-X (Shimizu, Co., Ltd., Osaka, Japan), which contains poly (acrylic acid) (PAAH) with excess base to make it water soluble by deprotonation of the acidic groups, and a +2.0 V dc potential was applied between the optical fiber and a Pt coil for 5 s to oxidize H_2O ($2\ H_2O \rightarrow O_2 + 4H^+ + 4e^-$) at the fiber. PPA^- at the electrode surface was protonated, resulting in the precipitation of an insulating PAAH layer on the electrode. The insulated electrode was then removed from solution and cured in oven at 80^{o}C for 20 min and then at 150^{o}C for 30 min. The insulating layer shrank during curing step so that the sharp end of tip was exposed (Fig. 2.6).

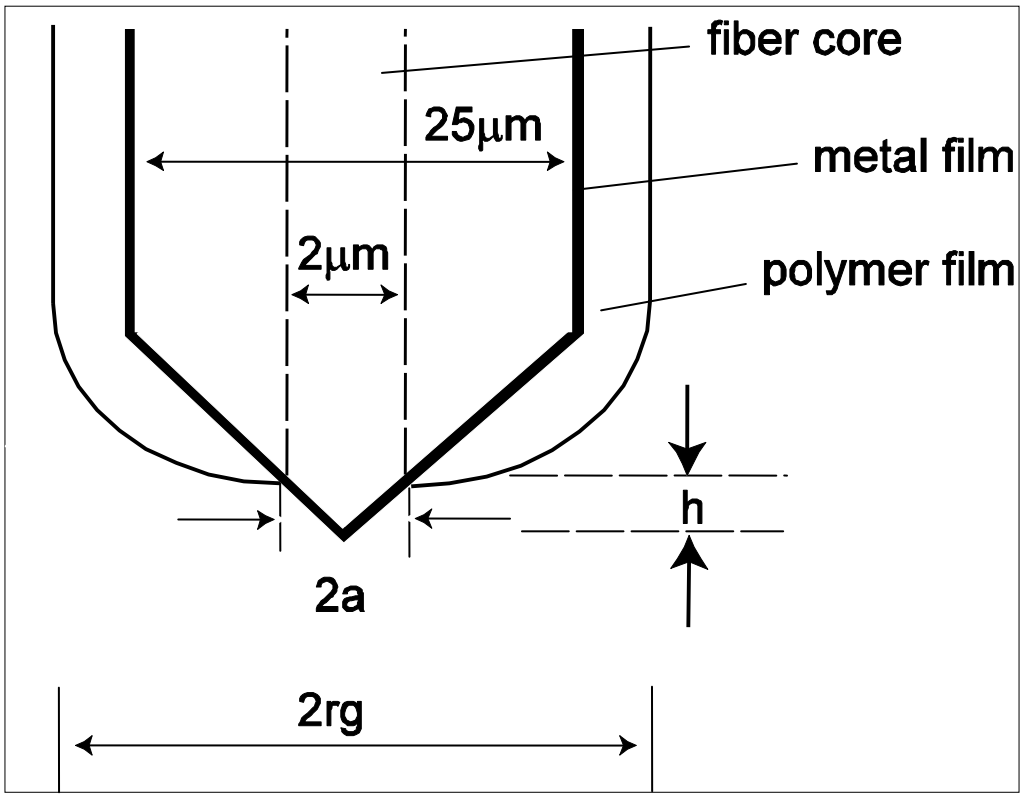

Figure 2.6. Electrode profile

2.4.3 Electrochemical Measurements

For electrochemical measurements, a two-electrode system was used. The working electrode was the prepared tip and the quasi-reference electrode was a silver wire. A CH Instruments (Austin, TX, USA) model 600A and a home-built SECM were used for all electrochemical measurements. In SECM approach curve experiments, the prepared tip was brought to a substrate surface by a set of x, y, z stages (M-462, Newport Corp., CA, USA) and a piezoelectric positioner and controller (models P621.ZCD and E621SR, Physik Instrumente, Germany) to give smooth movement in the direction perpendicular to the surface. Flat glass, polychlorotrifluoroethylene and Pt were used as substrates for SECM experiments.

2.5 RESULTS AND DISCUSSION

2.5.1 Fabrication of Conical Probes based on Selectively Etched Optical Fibers and Characterization by SEM

The multistep index optical fibers were etched in a NH_4F/HF buffer solution and used as a template of conical microelectrodes. The composition of the etching solution was adjusted so that the GeO_2-doped fiber core and the inner pure silica cladding were etched at the same speed while the outer F-doped cladding was etched faster. Actually, right after 60 min of etching, the outer cladding layer became much thinner (Fig. 2.7) and the ensemble of fiber core and inner cladding looked like a trapezoid. After 80 min, the outer cladding had been completely etched off and a sharp tip was formed (Fig. 2.8). In SECM applications, using selectively etched multistep index fibers has advantages over fibers with GeO_2-doped core and a single cladding layer[9, 19, 20] in that it has smaller tip size (~ 25 μm in outer diameter), which makes it possible to bring the tip closer to the substrate. We also noticed that the temperature played an important role on the etching speed; even one degree increase of the temperature would increase the etching rate in 70 nm/min.

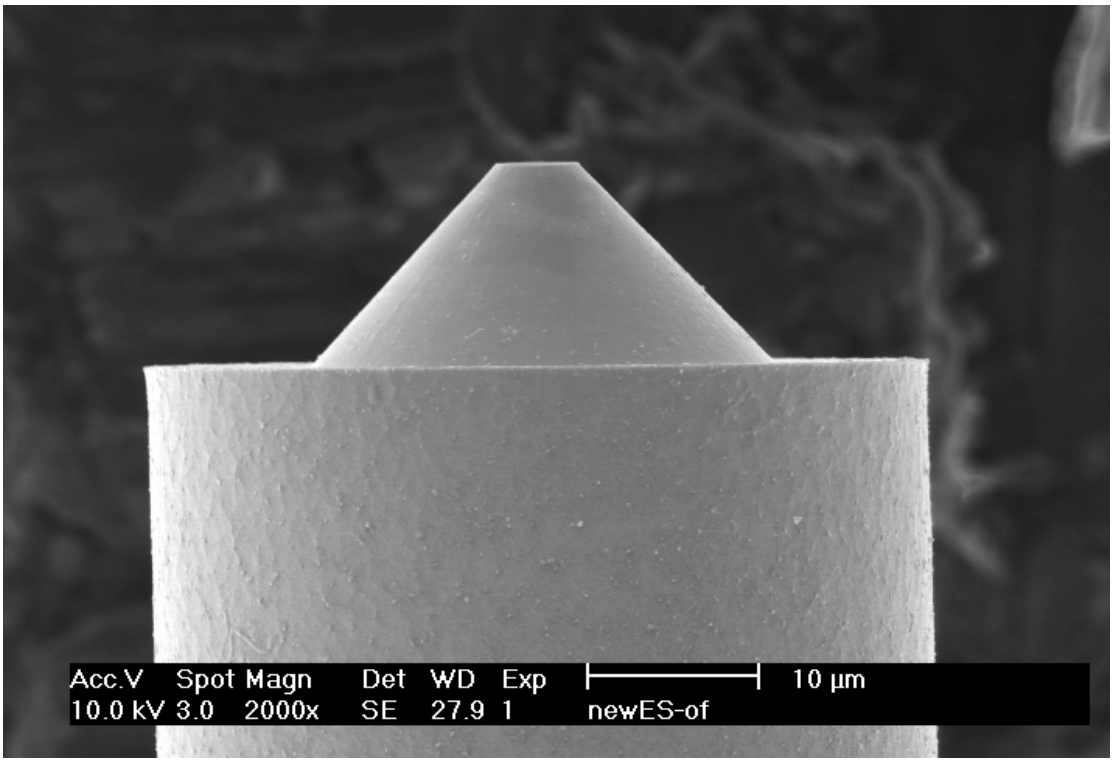

Figure 2.7 SEM image of selectively etched optical fibers after etching for 60min.

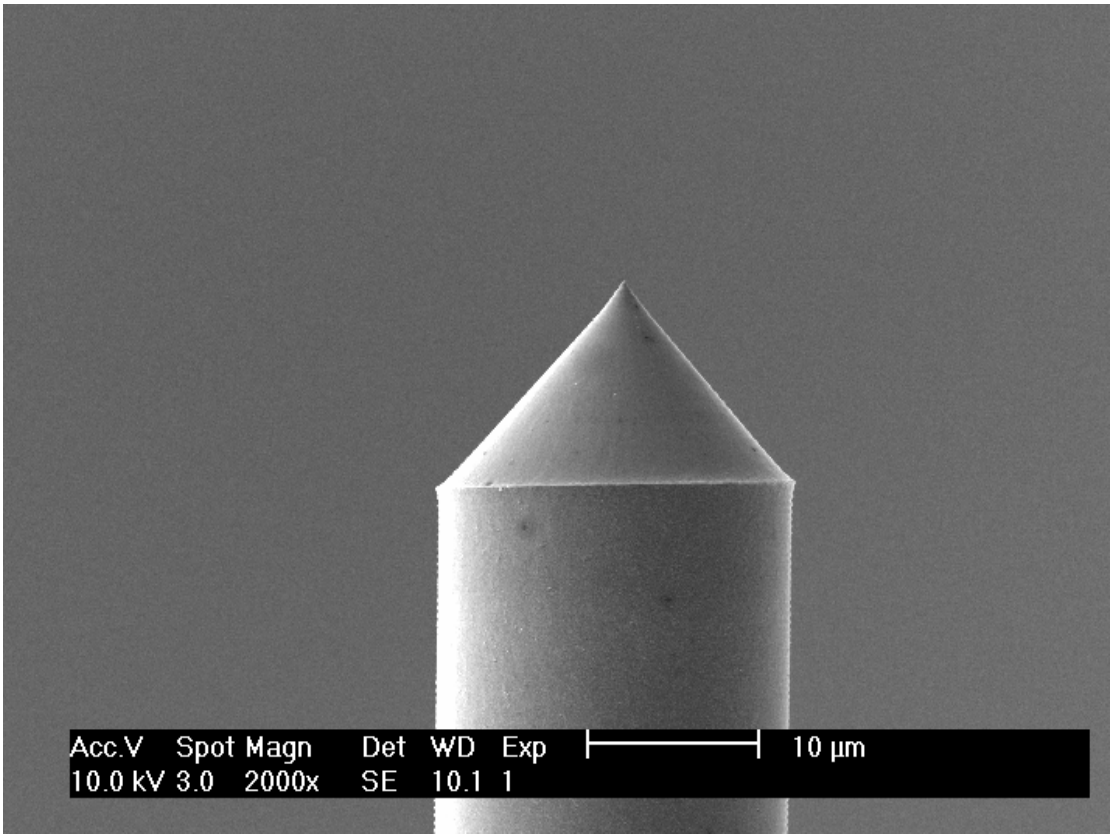

Figure 2.8 SEM image of selectively etched optical fibers after etching for 80min.

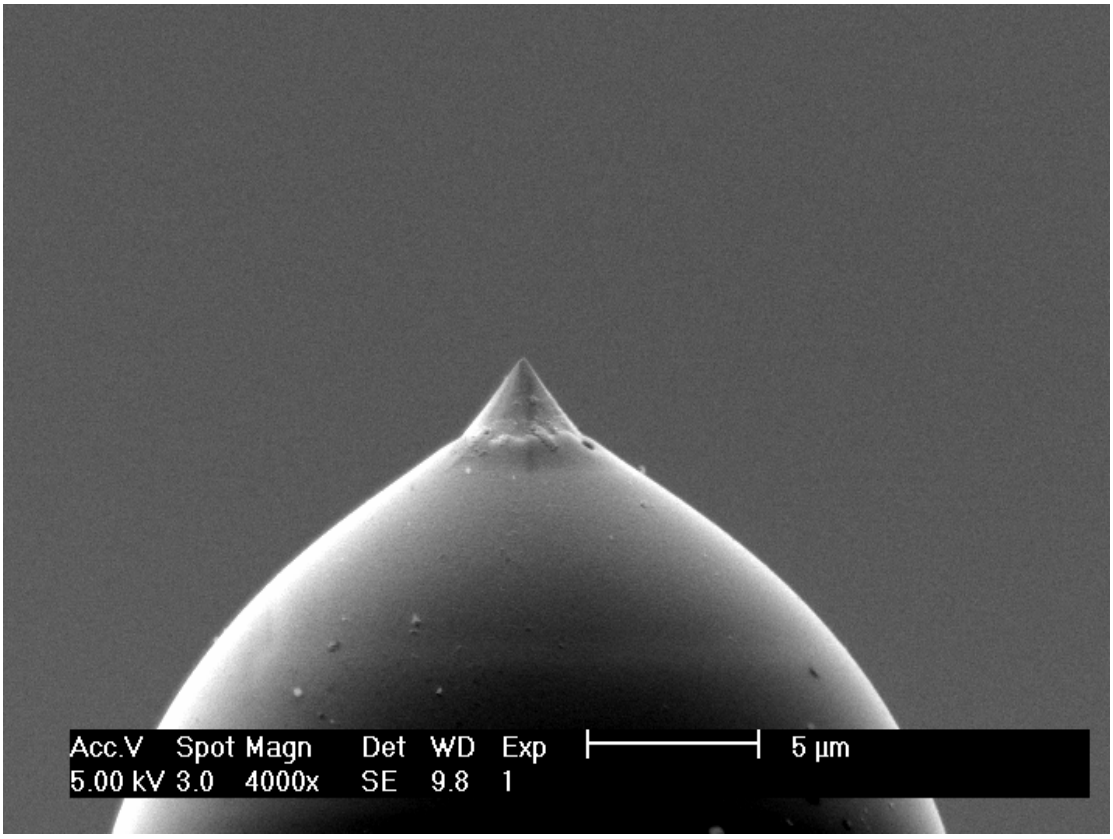

Figure 2.9 SEM image of a conical electrode after insulation.

An etched fiber was coated with gold by sputtering and then insulated with electrophoretic paint. Fig. 2.9 shows the SEM image of a conical probe after insulation. The image clearly shows a conical protrusion, which corresponds to the exposed gold tip. EDAX analysis was carried out to make sure that the protruding part was indeed the exposed gold tip as confirmed by EDAX spectrum.

2.5.2 Steady-state Cyclic Voltammetry

Exposition of a gold layer after deposition of electrophoretic paint was also confirmed by cyclic voltammetry carried out in a 1 mM 1,1′-ferrocenedimethanol/ 0.1 M KCl aqueous solution. The cyclic voltammogram obtained with the prepared tip is shown in Fig. 2.10. Typically, a well defined sigmoidal cyclic voltammogram of a good-quality UME was obtained with a selectively etched conical probe insulated by electrophoretic paint. The diffusion-limited steady-state current at a conical electrodes in a bulk solution, $i_{T,\infty}$, can be expressed as

$$i_{T,\infty} = nFDc_o ax, \qquad (12)$$

where F is the Faraday constant, D is the diffusion coefficient of the mediator, and x is a geometric factor depending on the shape of the electrode. With the geometry defined in Fig. 2.1, a value of 6.74 was obtained for the geometry factor, x, using numerical simulations at a large tip-current separation (d=100a). With the diffusion coefficient of 1,1′-ferrocenedimethanol (6.9×10^{-6} cm^2/s) determined by chronoamperometry at a 10 μm Pt microelectrode,[21, 22] the base radius, a, was calculated to be 1.0 μm according to Eq. 12 with $i_{T,\infty}$ of 0.470 nA.

However, only with cyclic voltammetry, it is not enough to confirm the profile of the prepared probes.[23] There are 3 independent parameters which decide the geometry and size of the conical probes, i.e., the base radius, height of the conical tip and the shape of the insulating sheath. Also there might be pinholes exposed other than the tip.

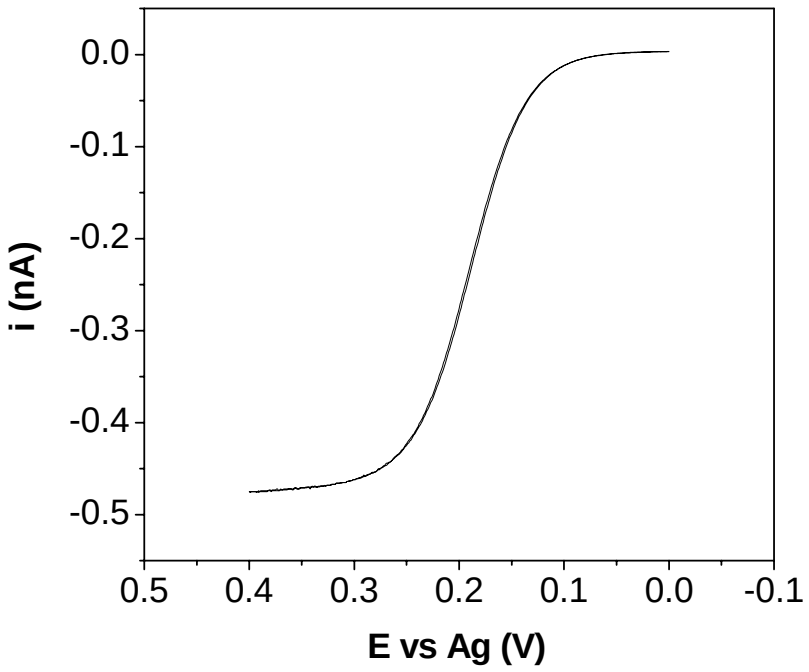

Figure 2.10 Cyclic votammogram from a conical probe in a aqueous solution of 1mM 1,1′-ferrocenedimethanol and 0.1 M KCl. Scan rate, 0.01 V/s.

2.5.3 SECM Approach Curve Measurements

Scanning electrochemical microscopy (SECM) approach curves were measured for further characterization of the electrode size and geometry. SECM approach curves depend on the size and geometry of the probes so that they are used to characterize disk,[24] conical,[10, 25] spherical,[26, 27] hemispherical[28, 29] and ring electrodes.[30] The SECM approach at a Pt substrate was measured with the same conical probe for cyclic voltammetry in Fig. 2.11. The tip potential was kept at 0.35 V where the oxidation of 1,1′-ferrocenedimethanol is diffusion limited and the probe was brought to the Pt surface at the speed of 1.0 μm/s. As the electrode moved toward the Pt substrate, the tip current increased gradually to 1.8 times of $i_{T,\infty}$ and then rapidly to more than 270 times of it (Fig 2.11a). The rapid increase is due to the contact between the tip and the substrate, where the active electrode area increases from the conical tip to the whole Pt substrate. This result confirms that the electrode tip is protruding from the insulating layer; otherwise, the insulating layer would touch the surface before the metal surface of the electrode touches it because even a slight tilt will cause the tip not moving vertically to the substrate. Fig. 2.11b also shows a theoretical SECM approach curve of a disk-shaped electrode (RG=2). Compared to disk electrode (h=0), conical electrode must approach closer to the substrate to reach a similar value of feedback current for a conductive substrate. The reason for the relatively smaller feedback at conical electrode with conductive substrates can be explained as follows: Far from the substrate, the diffusion to the UME tip achieves a spherical diffusion layer, whose dimensions are predominately determined by the base radius *a*, so the behavior is rather disk-like. However, when the tip approaches very close to the substrate, the diffusion layer is disturbed by the substrate before reaching a spherical diffusion layer and the dimensions of the diffusion layer are largely depend on the aspect ratio (h/a) or the tip angle of the conical tip. The experimental curve agrees very well with the theoretical one (Fig 2.11b), giving a =1.0 μm and h= 1.2 μm. This good agreement also confirms the electrode geometry as defined in Fig 2.1.

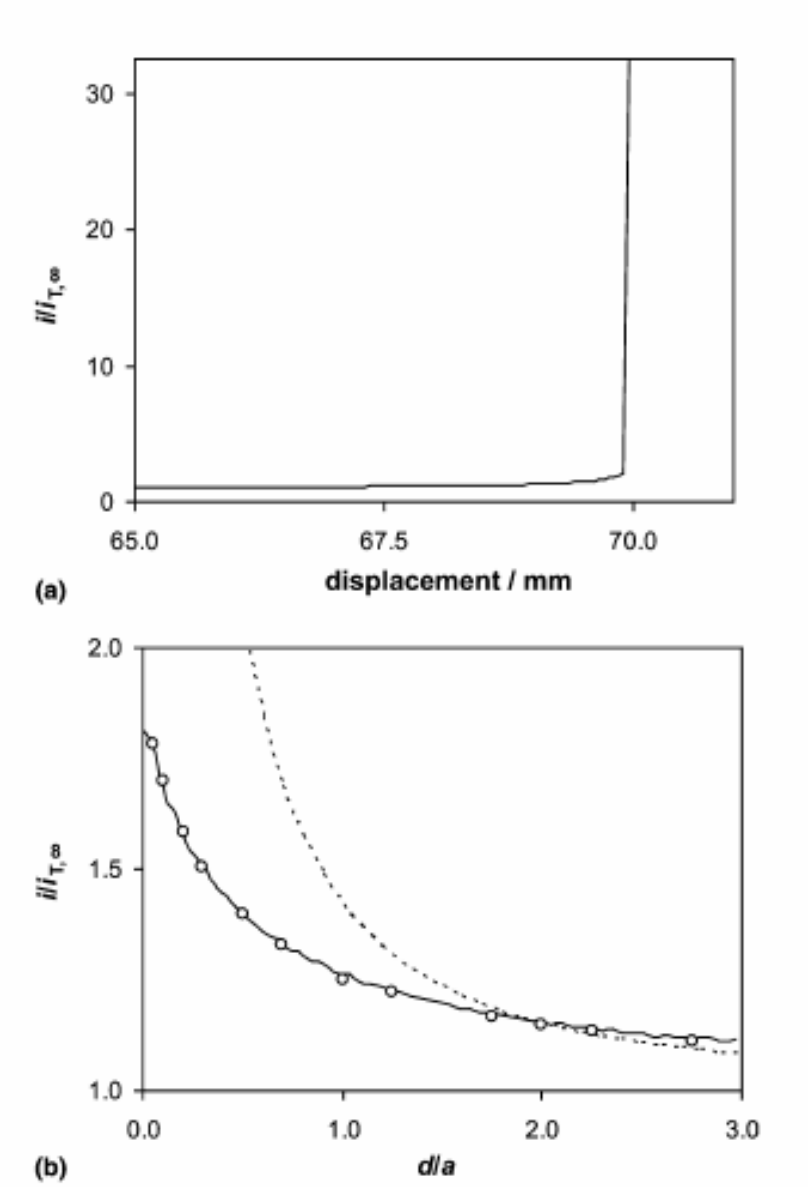

Figure 2.11 Experimental SECM approach curve (solid line) at a Pt substrate as obtained with the conical microelectrode used for cyclic voltammetry in Fig. 2.10. Solution contained 1 mM 1, 1'-ferrocenedimethanol and 0.1 M KCl in water. The circles represent the theoretical curve for a conical electrode with the tip angle of 80° (See Fig. 2.1 for the insulating layer geometry). The dotted line represents an approach curve of a disk-shaped electrode, where the disk radius and the outer radius of the insulating layer are *a* and 2*a*, respectively.

The electrode geometry and size were further confirmed by SECM approach curve experiments at an insulating substrate. Fig. 2.12a shows an experimental approach curve at a polychlorotrifluoroethylene substrate. The curve was obtained with the same probe as used for cyclic voltammertric and SECM positive feedback measurements in Fig.2.10 and Fig. 2.11b. As the electrode moved to the insulating substrate, the tip current decreased to 48% of $i_{T,\infty}$. Compared to the theoretical approach curve by a disk electrode over an insulating substrate also shown in Fig. 2.12b, the SECM feedback response for a conical probe needs to approach closer than a disk one in order to get the same level decrease of tip current. When the conical probe is positioned close to the insulating substrate, the substrate hinders the diffusion of the mediator from the bulk solution to the electrode surface so that the tip current decreases to a value lower than $i_{T,\infty}$. The experimental curve fits well with the theoretical one based on the geometry defined in Fig. 2.1 until the current decreases to 65% of $i_{T,\infty}$. The base radius was determined to be 1.0 μm, which agrees well with the value determined by cyclic voltammetry and the SECM approach experiment at a Pt substrate. However, the tip current decreased further. The final current value varies among electrodes in the range between 48% of $i_{T,\infty}$ and almost 0 as observed with a smaller electrode (a = 0.44 μm). We observed the further decrease of tip current with freshly prepared tips, which excludes the possibility of geometry changes on the tips dues to the contact with the tips and substrate by previous experiments. Meanwhile, the tip current over a glass substrate did not decrease to lower than 65% of $i_{T,\infty}$. Fig 2.12b shows an approach curve over a glass substrate at another conical electrode (a =0.70 μm). This result indicates that the further decrease of the tip current lower than 65% of $i_{T,\infty}$ is cause by the penetration of the conical tip into the soft polymer substrate. The penetration effect on the approach curve not only shows the robustness of the conical probe but also is important in interpreting SECM approach curves at a sharp probe over a soft substrate such as biological samples.

Finally, it should be note that both negative and positive feedback effects at conical electrodes are much smaller than those at disk-like ones (Figs. 2.11b, 2.12). This result indicates that, at a short tip-substrate distance, the tip current at conical electrodes is mainly controlled by diffusion of mediator through the gap between the tip and the substrate. The space domain of the gap is determined not only by the geometry of the insulating layer but also by the tip angle. A smaller feedback is expected with a sharper conical electrode.[10, 11, 25]

2.5.4 SECM Approach Measurements at Smaller Electrodes

Simulations with modified geometry (R=0.156a) as shown in Fig. 2.4 was applied for smaller electrode (a < 500 nm). The fitting of the experimental approach curves and theoretical ones are shown in Fig. 2.12. It has been noticed that, at smaller electrodes, deviations appear between experimental curves and theoretical one with the simulation based on Fig. 2.1. Experimental data agree very well with simulation taking into account the sharpness effect (geometry shown in Fig. 2.4) and this confirms that the tip is very sharp: ~ 80 nm in diameter for a conical electrode with base radius of 255 nm (Fig. 2.13).

2.5.5 Insulation with Electrophoretic Paint by Multiple Coating

The smallest electrode we can prepare by one-time insulation with electrophoretic paint is 255 nm in radius. White's group has reported fabrication of quasi-hemispherical nano-electrodes from etched Pt wires by electrophoretic paint method.[23] They fabricated electrodes with apparent radii in the range of 2-150 nm by repeated applications of polymer layers. We used a slightly modified version of their electrophoretic paint method. We used the original polymer solution for the first deposition of electrophoretic paint. After insulation, we checked the electrode size by steady-state cyclic voltammetry. Depending on the size of the electrode, we repeated the electrophoretic paint coating by a 1:1 (volume ratio) diluted polymer solution. Fig. 2.14 shows the steady-state cyclic voltammograms of electrodes prepared by multiple polymer coating. Assuming the electrode maintains its conical shape, we calculated the electrode radius by Eq. 12 to be 180 (Fig. 2.14a) and 100 nm (Fig. 2.14b), respectively. Because it's not enough to confirm the size and geometry of the prepared electrode with only cyclic voltammetry, we also characterized it with SECM. Unfortunately, we couldn't obtain apparent feedback changes by approaching the electrode to both an insulating substrate and a conductor.

It seems that the metal coated part of the electrode is not protruding from the insulating layer. And from the SEM image (Fig. 2.15) taken from an electrode with multiple polymer coatings, it looks more like a recessed electrode. From our results, we also found repeatedly coating polymer is not very controllable and reproducible. Therefore, it is necessary for us to find another option to fabricate nano-probes.

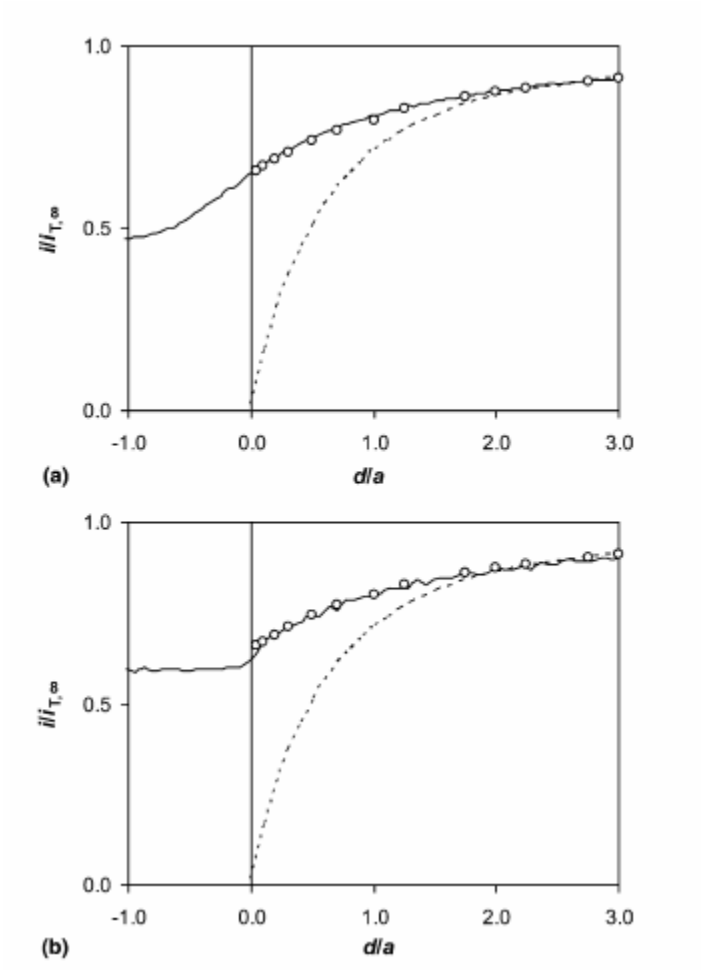

Figure 2.12 Experimental approach curves (solid lines) (a) over a polychlorotrifluoroethylene substrate at the same probe as used for Figs. 2.10 and 2.11 and (b) over a glass substrate at a conical electrode with the base radius of 0.70 μm. Solution contained 1 mM 1, 1'-ferrocenedimethanol and 0.1 M KCl in water. The circles represent the theoretical curve for a conical electrode with the tip angle of 80° (see Fig. 2.1 for the insulating layer geometry). The dotted lines represent an approach curve of a disk-shaped electrode, where the disk radius and the outer radius of the insulating layer are a and $2a$, respectively.

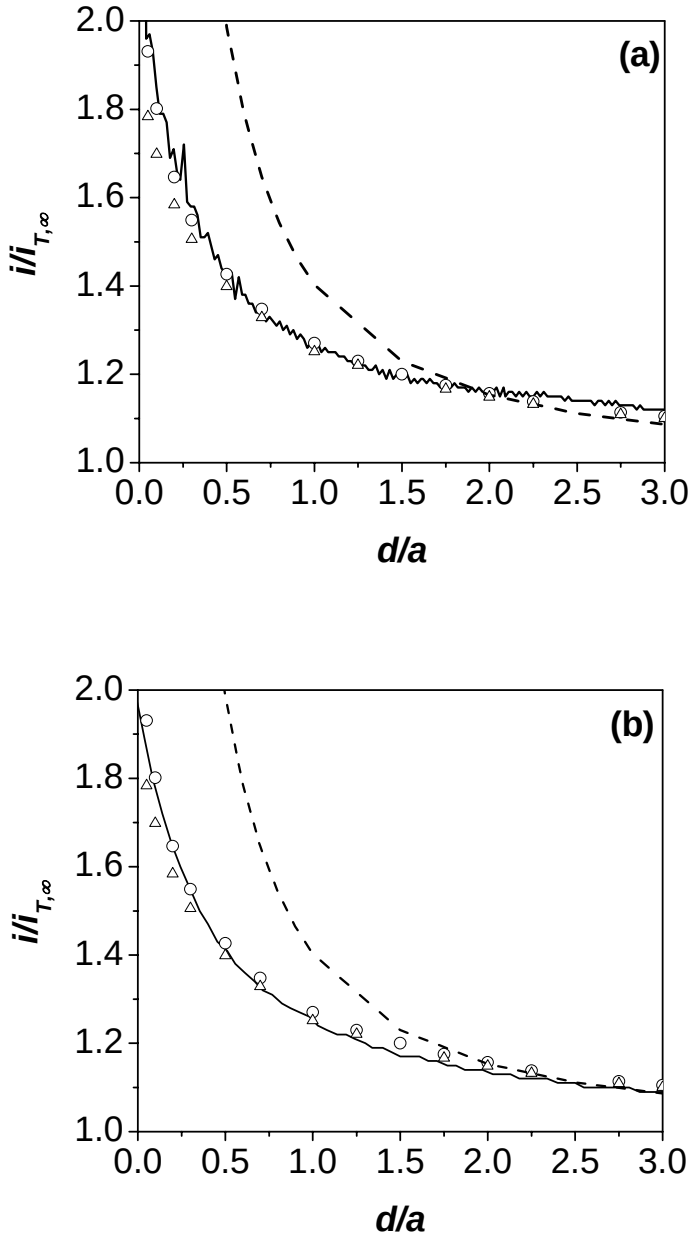

Figure 2.13 Comparison of theoretical (circles) and experimental SECM (solid line) curves at a Pt substrate for conical electrodes with base radius: (a) 255 nm and (b) 382 nm. The geometry for simulation is based on Fig. 2.4 with R=0.156a. The dashed line represents a theoretical approach curve of a disk-like electrode with RG=2. Triangles represent theoretical approach curve at a conical electrode with geometry defined in Fig. 2.1. Solution contained 1 mM 1,1′-ferrocenedimethanol and 0.1 M KCl in water.

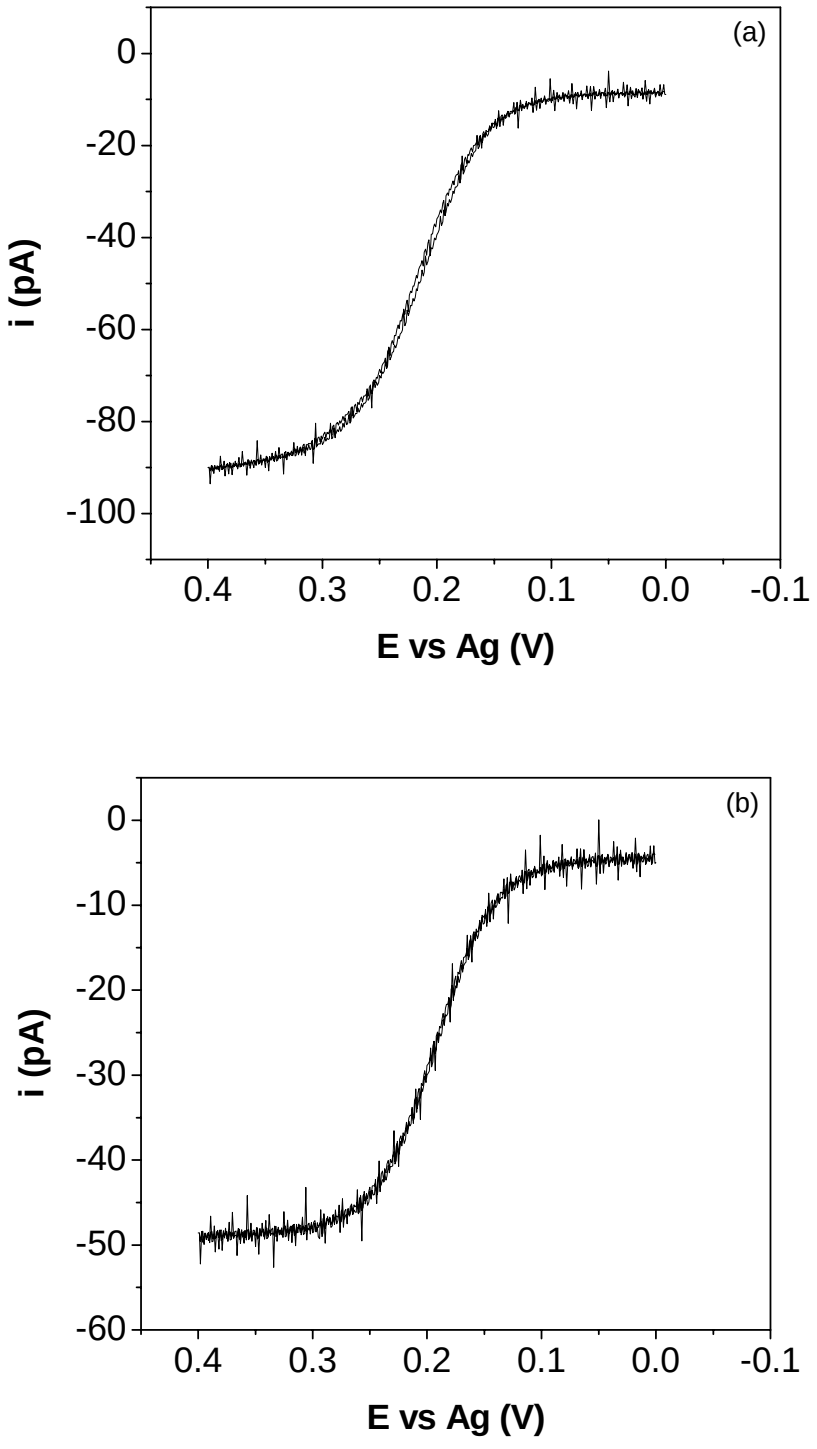

Figure 2.14 Cyclic votammogram from probes prepared by repeated polymer applications in an aqueous solution of 1 mM 1,1′-ferrocenedimethanol and 0.1 KCl. Scan rate 0.01 V/s.

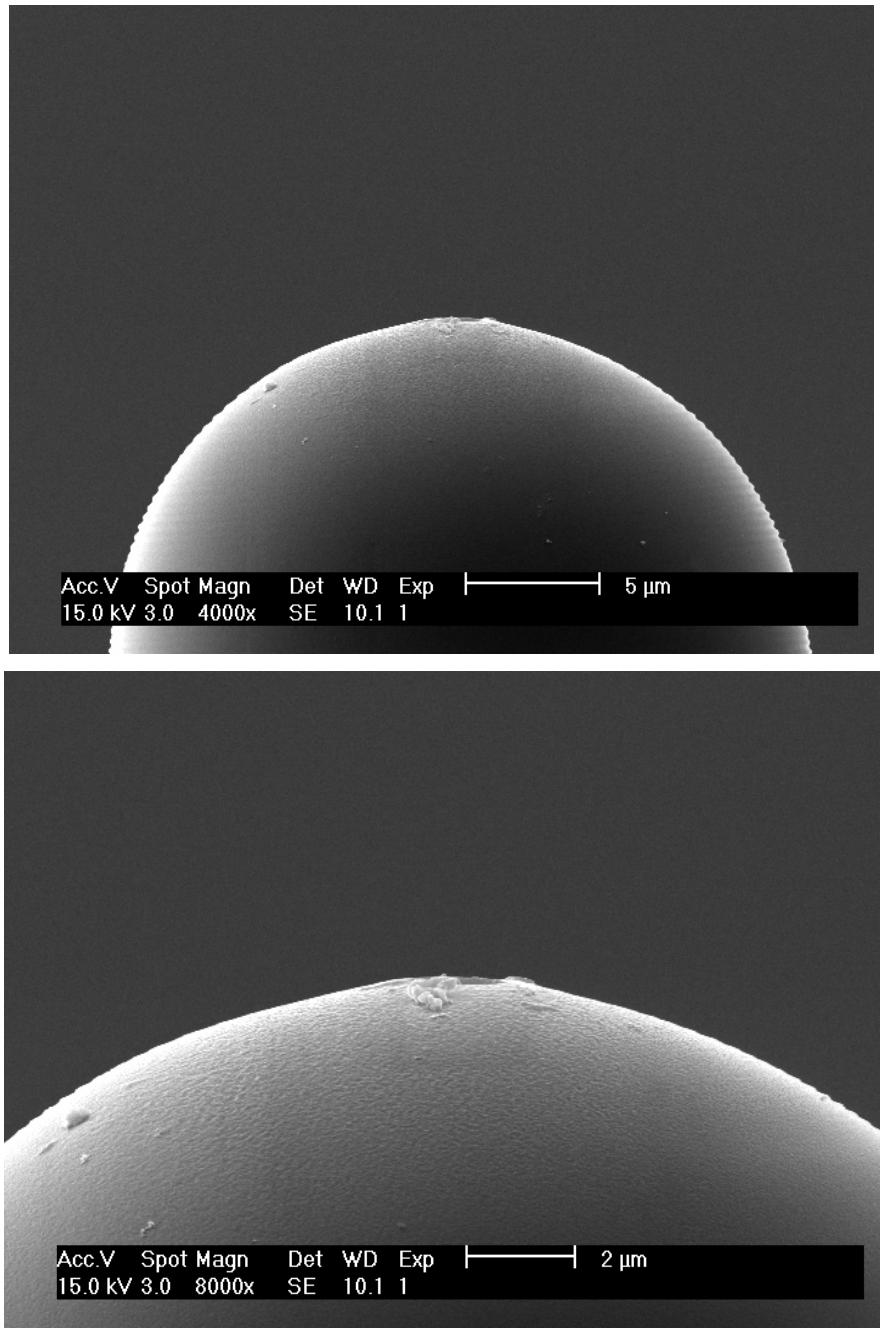

Figure 2.15 SEM images of a probe prepared by repeated polymer applications.

2.5.6 Gold Quality of the Electrodes

During our experiments, we found out that sometime the electrode surface got “ugly” after sputtering of gold (Fig. 2.16b). The reason might be because the pressure of sputter coater 108 auto is not low enough (~ 1e-4 Torr) and the environment is too humid. So we decided to use the Perkin-Elmer 2400 6J sputtering instrument in the cleanroom of Carnegie Mellon University with the capacity of pressure as low as 1e-8 Torr.

2.6 CONCLUSIONS

Selectively etched optical fibers were used as a template of conical microelectrode. The gold coated tapered optical fibers were insulated with electrophoretic paint leaving only tips exposed. The electrode geometry and size were determined by both steady-state cyclic voltammetry and SECM. The experimental approach curve data fit well with theoretical ones, yielding values in the range of 0.255-0.98 and 0.3-1.2 μm for the base radius and height of the conical probes, respectively. The aspect ratio of the conical tip corresponds to the tip angle of 80°, which is consistent with the tip angle of the tapered optical fiber determined by SEM. This result indicates the geometry of the conical electrode is well controlled by the selective etching technique. The etching technique also allows control of tip angle in the range between 14° and 180°.[9] And it is possible to construct smaller probes by varying the insulating procedure. However, a smaller feedback current will be observed for a conical probe with a smaller tip angle. Both SECM positive and negative feedback effects at the conical probes show that the tip current is mainly controlled by the gap between the tip and the substrate, namely, the domain defined by the tip angle and the insulating layer.

Multiple coating of electrophoretic paint results mostly recessed electrodes, which are not suitable for SECM applications. Further investigations on how to prepare electrodes with size smaller than 200 nm in radius will be discussed in chapter 3.

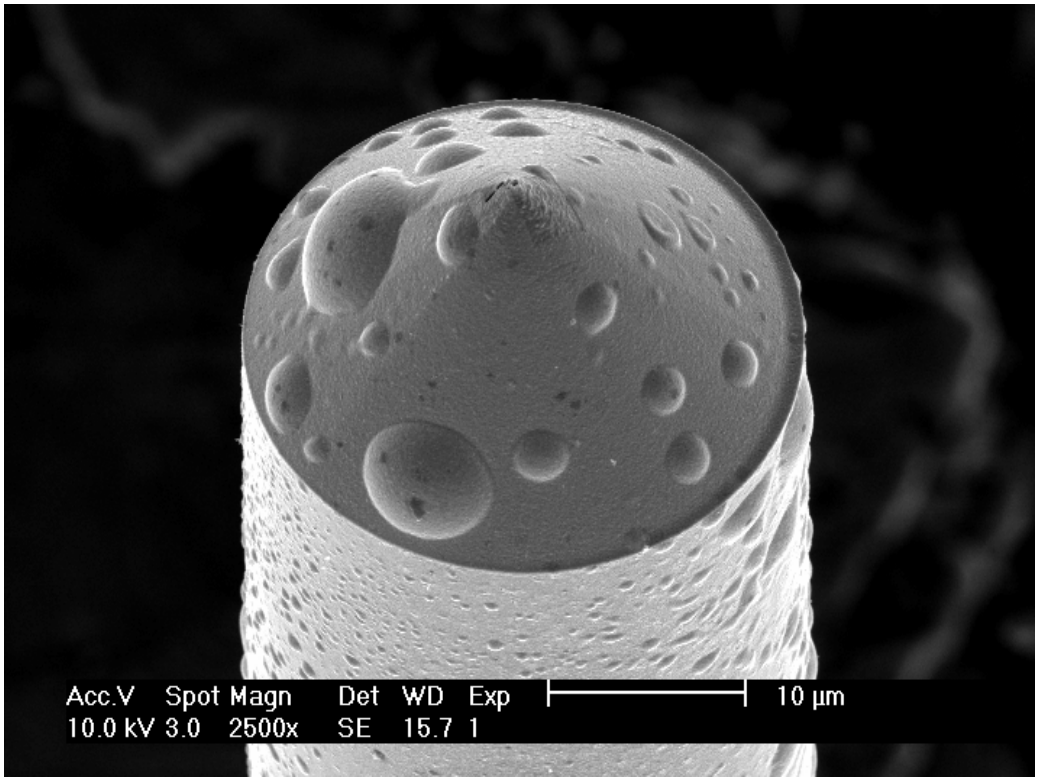

Figure 2.16 Electrode with bad gold coating.

2.7 REFERENCES

(1) Kuhn, L. S.; Weber, A.; Weber, S. G. *Analytical chemistry* **1990**, *62*, 1631-1636.

(2) Pennarun, G.; Boxall, C.; O'Hare, D. *Analyst (Cambridge, United Kingdom)* **1996**, *121*, 1779-1788.

(3) Casillas, N.; James, P.; Smyrl, W. H. *Journal of the Electrochemical Society* **1995**, *142*, L16-L18.

(4) James, P.; Casillas, N.; Smyrl, W. H. *Proceedings - Electrochemical Society* **1996**, *95-15*, 425-434.

(5) Lee, Y.; Bard, A. J. *Analytical Chemistry* **2002**, *74*, 3626-3633.

(6) Lee, Y.; Ding, Z. F.; Bard, A. J. *Analytical Chemistry* **2002**, *74*, 3634-3643.

(7) Betzig, E.; Trautman, J. K. *Science* **1992**, *257*, 189-195.

(8) Xiong, H.; Guo, J.; Kurihara, K.; Amemiya, S. *Electrochemistry Communications* **2004**, *6*, 615-620.

(9) Ohtsu, M.; Editor *Near-Field Nano/Atom Optics and Technology*, 1998.

(10) Mirkin, M. V.; Fan, F. R. F.; Bard, A. J. *Journal of Electroanalytical Chemistry* **1992**, *328*, 47-62.

(11) Fulian, Q.; Fisher, A. C.; Denuault, G. *Journal of Physical Chemistry B* **1999**, *103*, 4387-4392.

(12) Zoski, C. G.; Mirkin, M. V. *Analytical Chemistry* **2002**, *74*, 1986-1992.

(13) Mononobe, S.; Ohtsu, M. *IEEE Photonic. Technol. Lett.* **1998**, *10*, 99.

(14) Slevin, C. J.; Gray, N. J.; Macpherson, J. V.; Webb, M. A.; Unwin, P. R. *Electrochemistry Communications* **1999**, *1*, 282-288.

(15) Conyers, J. L.; White, H. S. *Analytical Chemistry* **2000**, *72*, 4441-4446.

(16) Bach, C. E.; Nichols, R. J.; Beckmann, W.; Meyer, H.; Schulte, A.; Besenhard, J. O.; Jannakoudakis, P. D. *Journal of the Electrochemical Society* **1993**, *140*, 1281-1284.

(17) Bach, C. E.; Nichols, R. J.; Meyer, H.; Besenhard, J. O. *Surface & Coatings Technology* **1994**, *67*, 139-144.

(18) Schulte, A.; Chow, R. H. *Analytical Chemistry* **1996**, *68*, 3054-3058.

(19) Burgos, P.; Lu, Z.; Ianoul, A.; Hnatovsky, C.; Viriot, M. L.; Johnston, L. J.; Taylor, R. S. *Journal of Microscopy (Oxford, United Kingdom)* **2003**, *211*, 37-47.

(20) Ianoul, A.; Burgos, P.; Lu, Z.; Taylor, R. S.; Johnston, L. J. *Langmuir* **2003**, *19*, 9246-9254.

(21) Denuault, G.; Mirkin, M. V.; Bard, A. J. *Journal of Electroanalytical Chemistry and Interfacial Electrochemistry* **1991**, *308*, 27-38.

(22) Hyk, W.; Nowicka, A.; Stojek, Z. *Analytical Chemistry* **2002**, *74*, 149-157.

(23) Watkins, J. J.; Chen, J. Y.; White, H. S.; Abruna, H. D.; Maisonhaute, E.; Amatore, C. *Analytical Chemistry* **2003**, *75*, 3962-3971.

(24) Kwak, J.; Bard, A. J. *Analytical Chemistry* **1989**, *61*, 1221-1227.

(25) Zoski, C. G.; Liu, B.; Bard, A. J. *Analytical Chemistry* **2004**, *76*, 3646-3654.

(26) Demaille, C.; Brust, M.; Tsionsky, M.; Bard, A. J. *Analytical Chemistry* **1997**, *69*, 2323-2328.

(27) Abbou, J.; Demaille, C.; Druet, M.; Moiroux, J. *Analytical Chemistry* **2002**, *74*, 6355-6363.

(28) Selzer, Y.; Mandler, D. *Analytical Chemistry* **2000**, *72*, 2383-2390.

(29) Mauzeroll, J.; Hueske, E. A.; Bard, A. J. *Analytical Chemistry* **2003**, *75*, 3880-3889.

(30) Lee, Y.; Amemiya, S.; Bard, A. J. *Analytical Chemistry* **2001**, *73*, 2261-2267.

3.0 FABRICATION AND CHARACTERIZATION OF NANO-PROBES FOR SECM

3.1 ABSTRACT

In order to fabricate electrodes within 200 nm in radius using selectively etched optical fiber as the template, we tried several approaches: (1) Using focused ion beam (FIB) milling we could cut the gold-coated tip at desired size with nanometer precision. However, after electrophoretic paint deposition on FIB modified fibers, the apparent size of the electrode increased against our expectation from FIB, which indicated that gold exposed not only at the tip but also on the side-wall. (2) Insulating gold-coated probes by sputtering silicon oxide is tested and still under investigation.

3.2 INTRODUCTION

In chapter 2, we introduced the fabrication of conical electrode for SECM by selective etching and electrophoretic paint techniques. It proved that the selectively etched optical fiber is a good template for reproducibly preparing sharp tips with defined geometry. We have succeeded in making well-defined and reproducible conical electrodes with radius as small as 255 nm. However, as we tried to fabricate even smaller electrode, electrophoretic paint technique didn't give us satisfactory results. By repeatedly depositing electrophoretic paint on the gold-coated fibers, we mostly obtained recessed electrodes, which is not good for SECM application. And the multiple-coating process is not controllable or reproducible to expose the probe tip smaller than submicrometer in diameter, which has also been mentioned by other researchers. [1]

FIB milling is a modern technique in designing and sculpturing nano- and micro-meter structures with high precision. This technique was mainly developed during the late 1970s and the early 1980s, and the first commercial instruments were introduced more than a decade ago.[2] The key ability of FIB technology is its capability to localize the modification to only the area requiring alternation. Because this technology enables localized milling with nanometer precision, we thought it would be a good attempt to apply FIB in modifying our selectively etched fiber probes.

If we insulate the fiber probes with electrophoretic paint prior to FIB milling, there are two possibilities (Fig. 3.1): (a) we completely insulate the tip and then cut an opening with FIB in nanometer size. However, we might get a probe with large RG because the insulating layer is quite thick (Fig. 2.16 in Chap 2). Nano-electrode with large RG in SECM is not good in that the tip can not approach the surface of the substrate very close to collect enough information before the insulating sheath touches the surface. Therefore, this is not a suitable way; (b) we insulate the fiber with only the tip exposed and then cut with FIB. This way the tip size is controlled by how well we expose the tip after electrophoretic paint not by FIB. So it is again not desirable. Then we thought about changing the order of FIB milling and electrophoretic paint insulation: Fig. 3.2 shows the schematic: the tip of gold-coated optical fiber is modified by FIB in submicrometer size and electrophoretic paint is applied on the FIB modified probes for insulation. In ideal situation, we would be able to fabricate nano-meter ring or disk electrode depending on where we locate the FIB milling window. Disk-like nanoelectrode is useful in SECM in measuring fast reactions in localized microenvironment. And ring-shaped nano-electrode by selectively etched optical fiber has the advantage in applications such as combined SECM/optical microscopy. If we can make such electrodes with defined geometry, they will be very useful in the above areas. There might be limitations too, such as we can not insulate the electrode perfectly as we desired.

Another option to prepare smaller electrode is as follows: sputter silicon oxide on gold-coated fibers and use FIB to modify the tip (Fig. 3.3). If we are able to control how well and how thick we can sputter silicon oxide on the gold-coated fibers, using FIB to mill the opening of silicon oxide insulated fiber seems quite promising in the sense of nano-electrode fabrication. Adjusting parameters for sputtering silicon oxide is still undergoing.

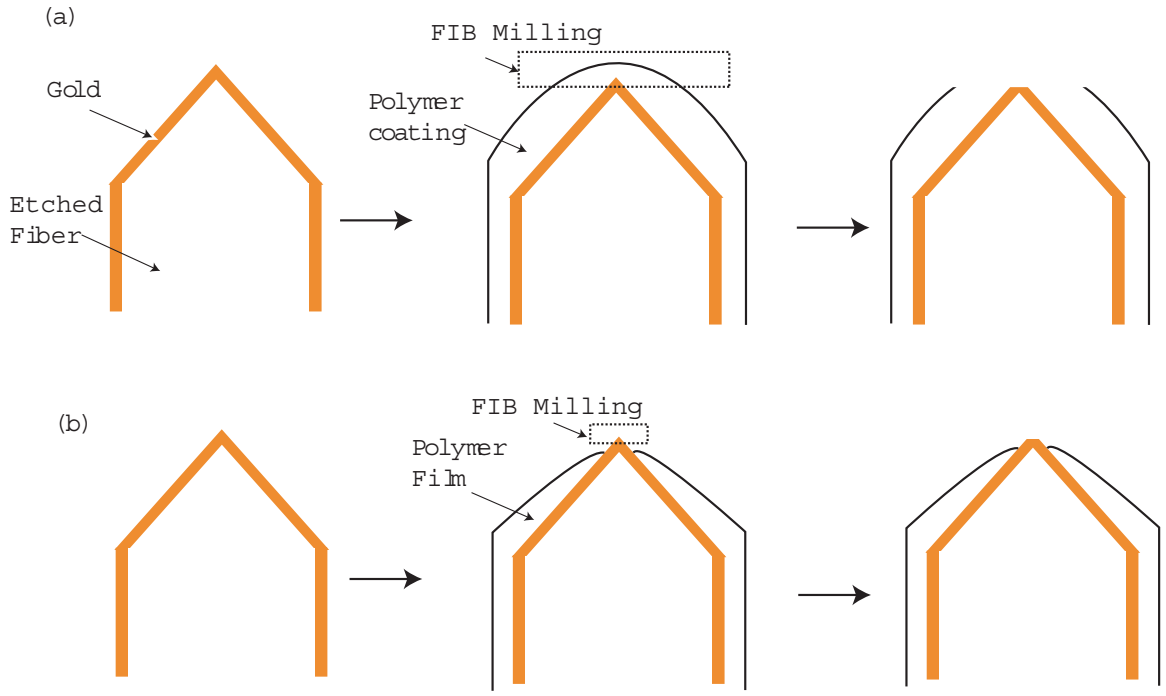

Figure 3.1 Schematic of FIB milling after electrophoretic paint insulation

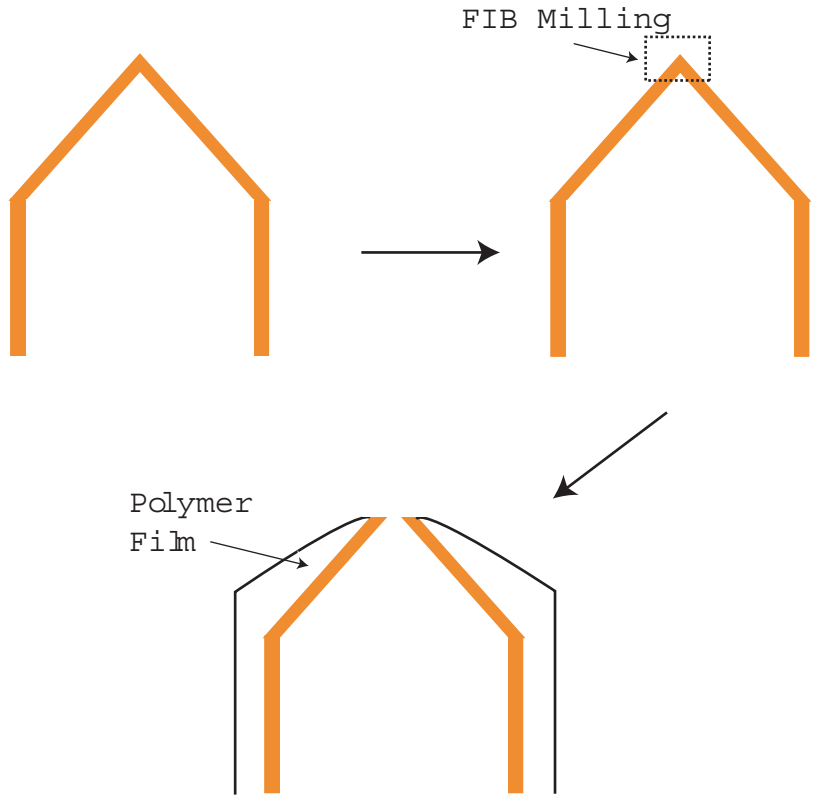

Figure 3.2 Schematic of FIB milling before electrophoretic paint insulation

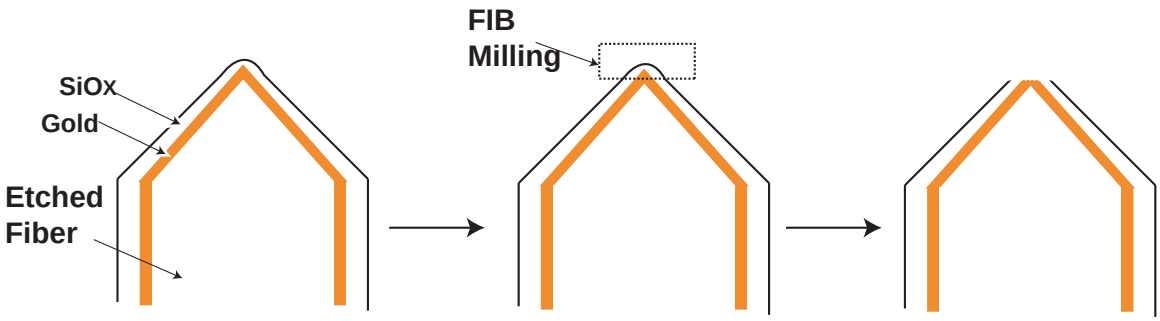

Figure 3.3 Schematic of nanoelectrode fabrication by sputtering of silicon oxide and FIB

3.3 EXPERIMENTAL

Chemicals, selective etching are the same as described in Chapter 2. All etching, focused ion beam milling and sputtering were carried out in the clean room at Carnegie Mellon university.

3.3.1 FIB Milling of the Selectively Etched Optical Fibers

To obtain a well-defined nanoelectrode, a FIB system (Micrion 2500 Focused Ion Beam System, Peabody, MA) was used. FIB system was used to image our samples with a 15μm and 1 pA beam with acceleration voltage of 50 kV and to mill openings with a resolution of 20 nm at the tips of the conical probes.

3.3.2 Insulating the Gold-Coated Selectively Etched Optical Fiber by Sputtering of SiO_x

Perkin Elmer 2400 6J Sputtering System was used to sputter a layer of Au (~ 100 nm) followed by an insulating layer of silicon oxide (SiO_x). A thin adhesion layer of Cr (~5 nm) was sputtered prior to SiO_x deposition. Optical fibers were mounted on a homemade stage or on a homemade rotator with 50 RPM. Silicon oxide was sputtered at different power (70 w ~ 250 w) from a RF-Diode target or a RF-Magnetron target.

3.4 RESULTS AND DISCUSSION

3.4.1 Focused Ion Bean Modification of SECM Probes

Fig. 3.4 shows the SEM images of a gold-coated conical fiber after FIB milling, both Au and silicon oxide were removed by FIB at the tip, and the size of the opening is consistent with expected milling size. This indicates that FIB technology is a reliable way to modify the size and geometry of our sample.

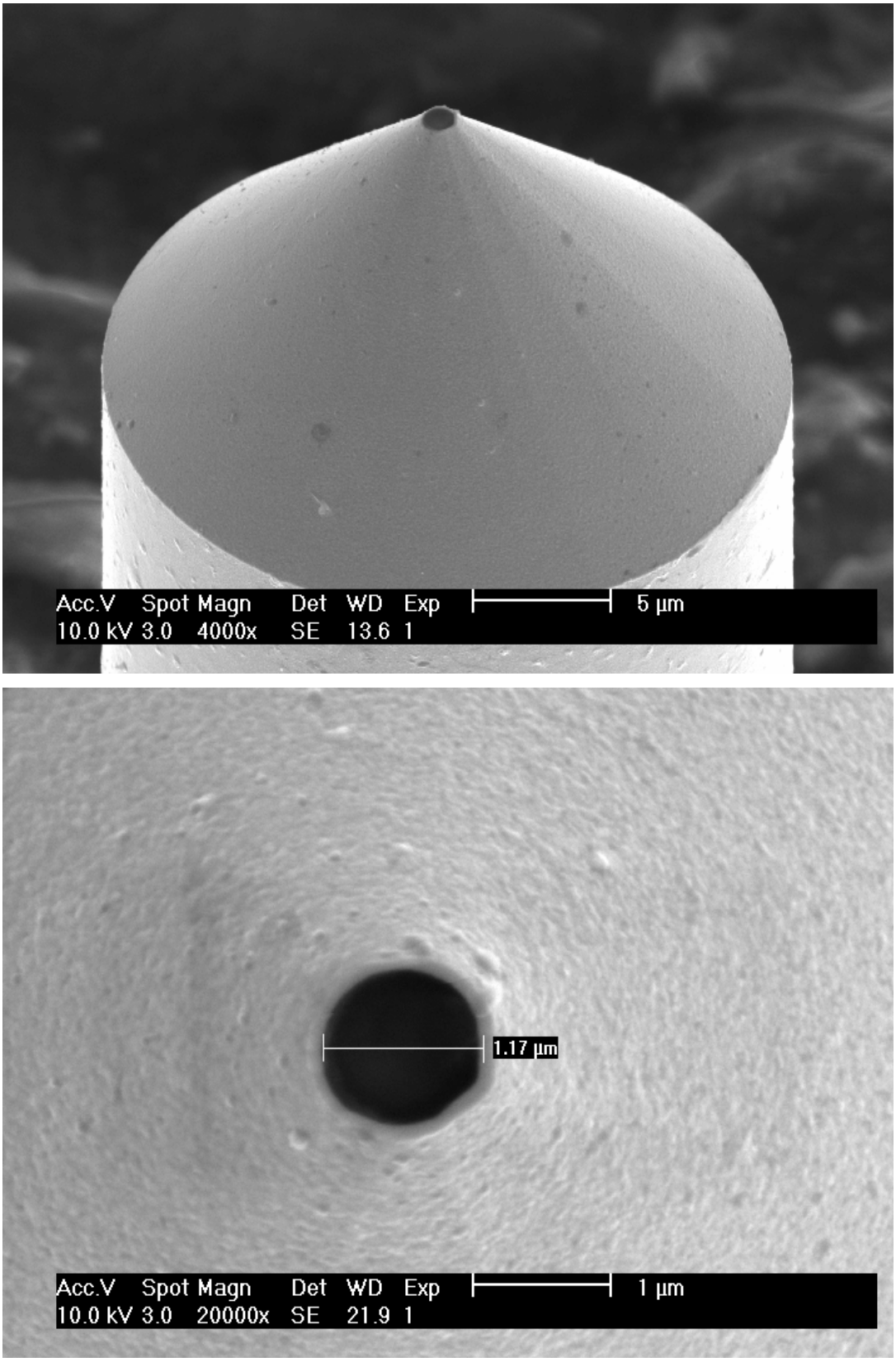

Figure 3.4 SEM images of a gold-coated probe modified by FIB

We then insulated FIB modified optical fiber probes with electrophoretic paint to characterize the tip electrochemically. Fig. 3.5 and Fig. 3.6 show the SEM images of a FIB modified fiber after electrophoretic paint insulation and the cyclic voltammogram of the same electrode. The cyclic voltammogram is very well-defined. However, we found out that the electrode's size is larger than the size we expected from a ring electrode based on the FIB milling. To address the possibility of pinhole effect, we measured currents by varying the depth of the probe in solution and we didn't find any significant difference, which excludes the possibility of pinholes. We also did SECM measurements on the same electrode to investigate its geometry. Fig. 3.7 shows the SECM approach curve. The experimental approach curve didn't fit with the theoretical one for ring electrode, which indicates the exact geometry of the probe is not ring-like. Our explanation of such disagreements is that gold was exposed not only at the tip but also at the wall of the conical slope so that we obtained smaller feedback compared to a ring electrode. Therefore, it seems not promising if we continue to use the electrophoretic paint technique for the insulation, because even though we can use FIB to modified the size at the tip of the electrode with nanometer precision, the final size of the electrode still becomes larger after electrophoretic paint deposition.

3.4.2 Insulating the Gold-Coated Selectively Etched Optical Fibers with Sputtering of SiO_x

Silicon oxide is commonly used in the micro-fabrication field as insulating material. We expected to sputter silicon oxide as an insulating layer on the gold-coated selectively etched optical fiber and then modify the size and geometry of the probe by FIB technology.

Fig. 3.8 shows the SEM images of fiber probes after sputtering silicon oxide with RF diode sputtering at 250 W. Evident damages on the fibers were noticed around the side wall of the fibers. We also tested the fiber probes electrochemically and didn't see any electric signal, which indicates the fiber probes were not electrically conducting after sputtering of silicon oxide.

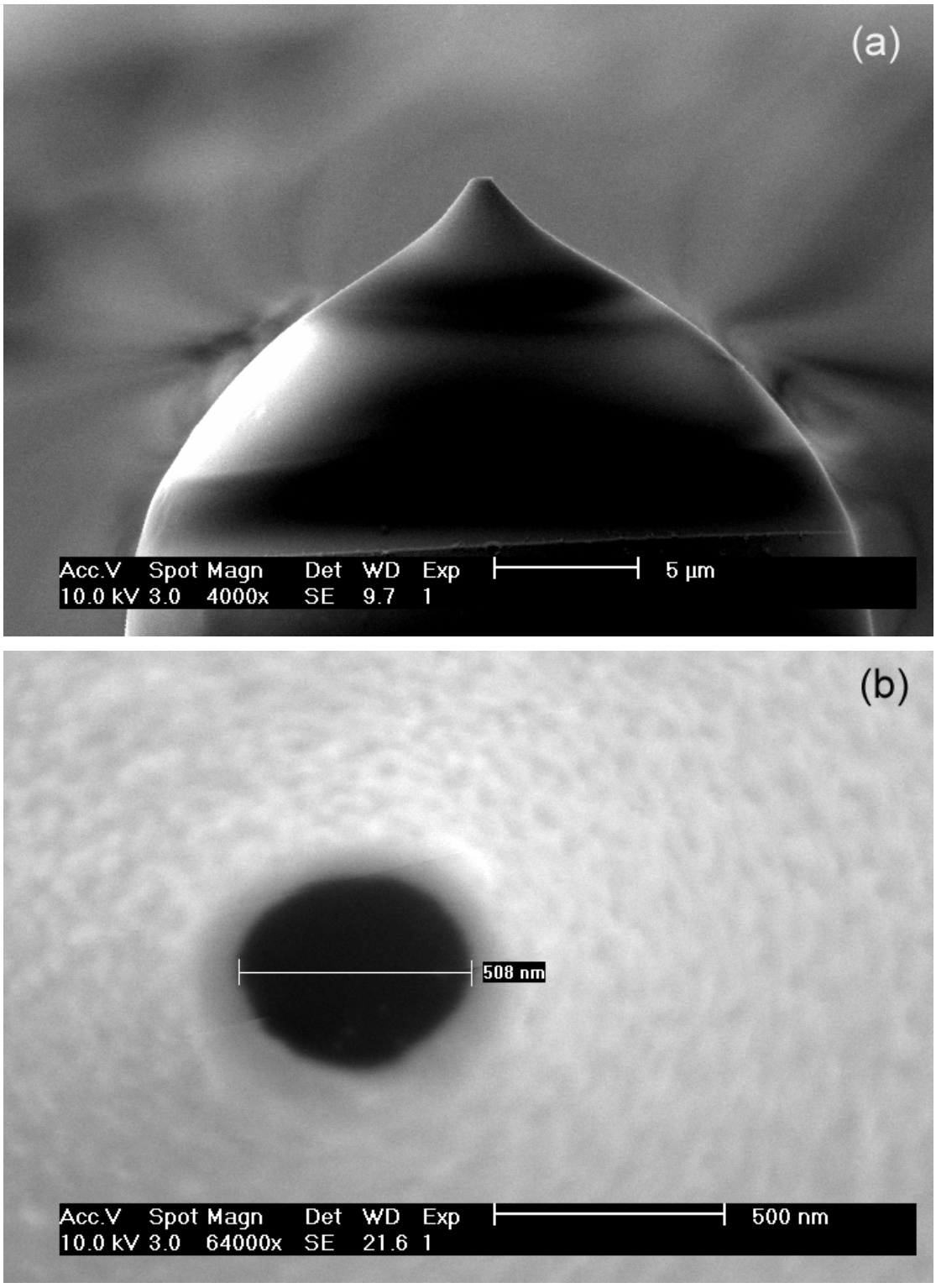

Figure 3.5 SEM images of a probe modified by FIB: (a) side view (b) top view.

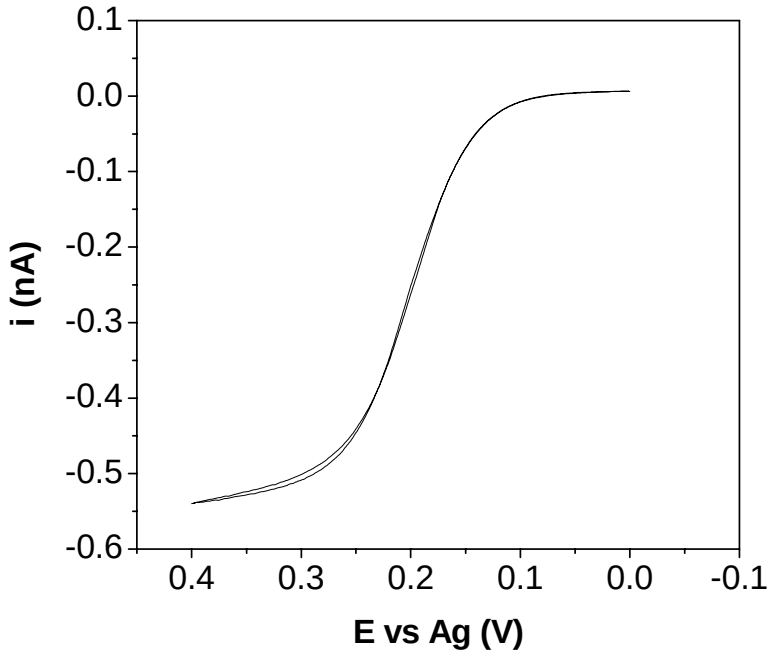

Figure 3.6 Cyclic votammogram from the electrode in Fig. 3.4 in an aqueous solution of 1 mM 1,1′-ferrocenedimethanol and 0.1 M KCl. Scan rate 0.01 V/s.

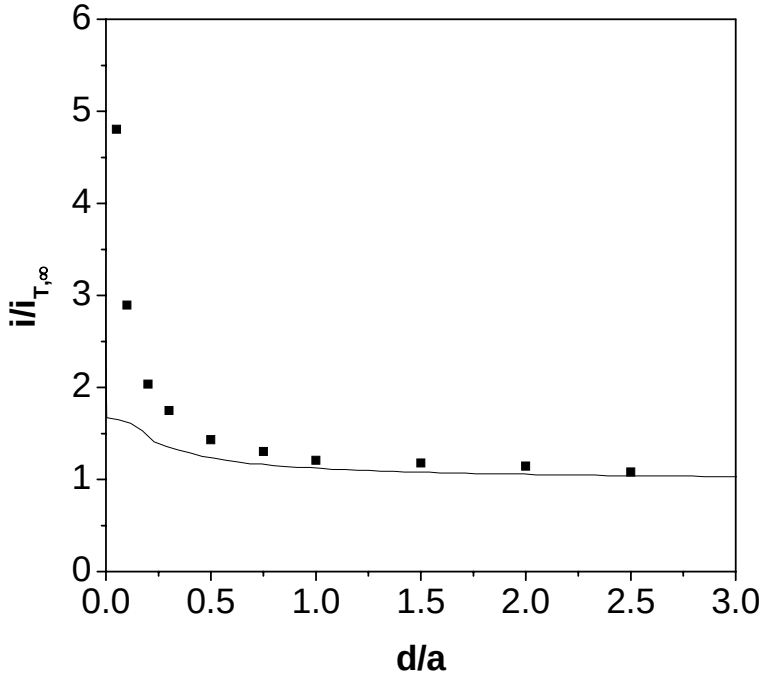

Figure 3.7 Comparison of experimental SECM curve (solid line) and theoretical (black square) curve (ring electrode, RG=1.5) at a Pt substrate for probe in Fig. 3.4. Solution contains 1 mM 1,1′-ferrocenedimethanol and 0.1 M KCl.

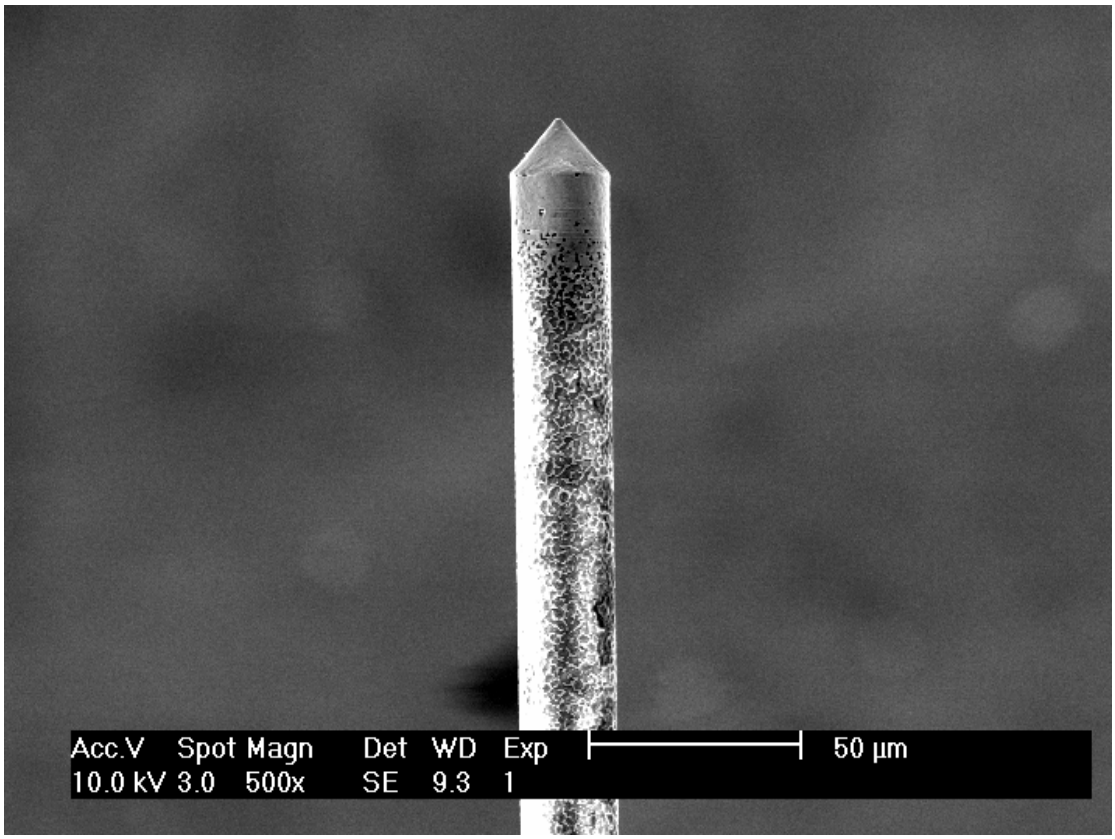

Figure 3.8 SEM image of a gold-coated probe after sputtering of silicon oxide with RF diode at 250 W.

We thought this damage might be due to the high power we applied, which will increase the sputtering temperature and in turn the surface tension between Au and silicon oxide layers. Therefore, we decided to decrease the power, but the problem was still not solved (Fig. 3.9). Then we decided to change the target to a magnetron sputtering source. A ring magnet below the target is used in the magnetron sputtering. Unlike rf diode, the secondary electrons in its field are trapped near the target and circulate near the target surface, which will form an extremely dense plasma. Under same condition, magnetron sputtering has higher efficiency and hence the deposition rate is higher. The advantage of magnetron sputtering allows us to sputter at a lower power with same deposition rate compared to rf diode, which could decrease the temperature induced by sputtering. Fig. 3.10 shows the SEM images of optical fiber probes prepared by magnetron sputtering, it seems that damages on the side wall are less. Also we could get electric signal from these probes. In order to verify if the electrode is insulated by the silicon oxide from sputtering, we tested the electrode electrochemically.

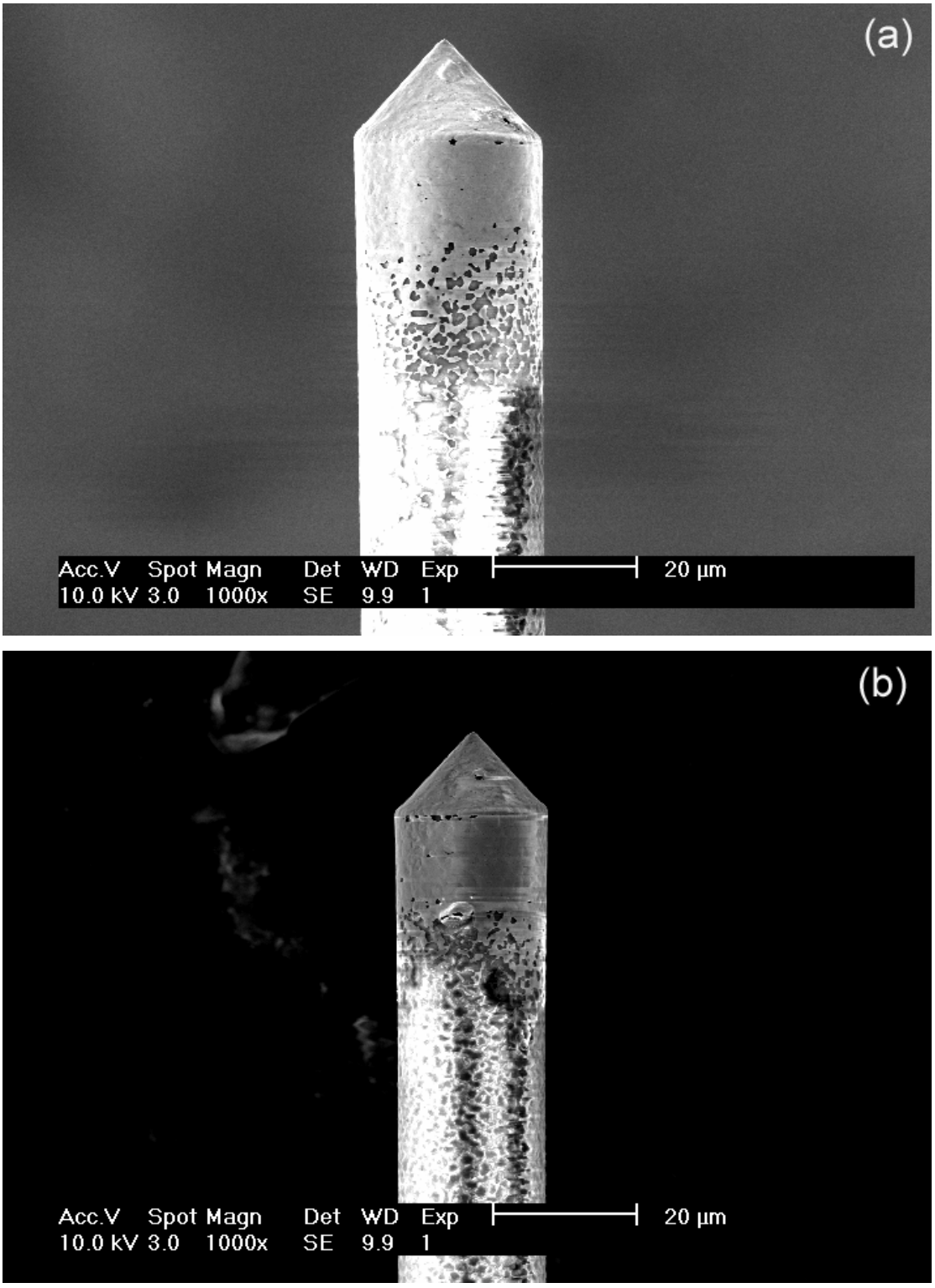

Figure 3.9 SEM image of a gold-coated probe after sputtering of silicon oxide with RF diode at: (a) 200 W and (b) 150 W

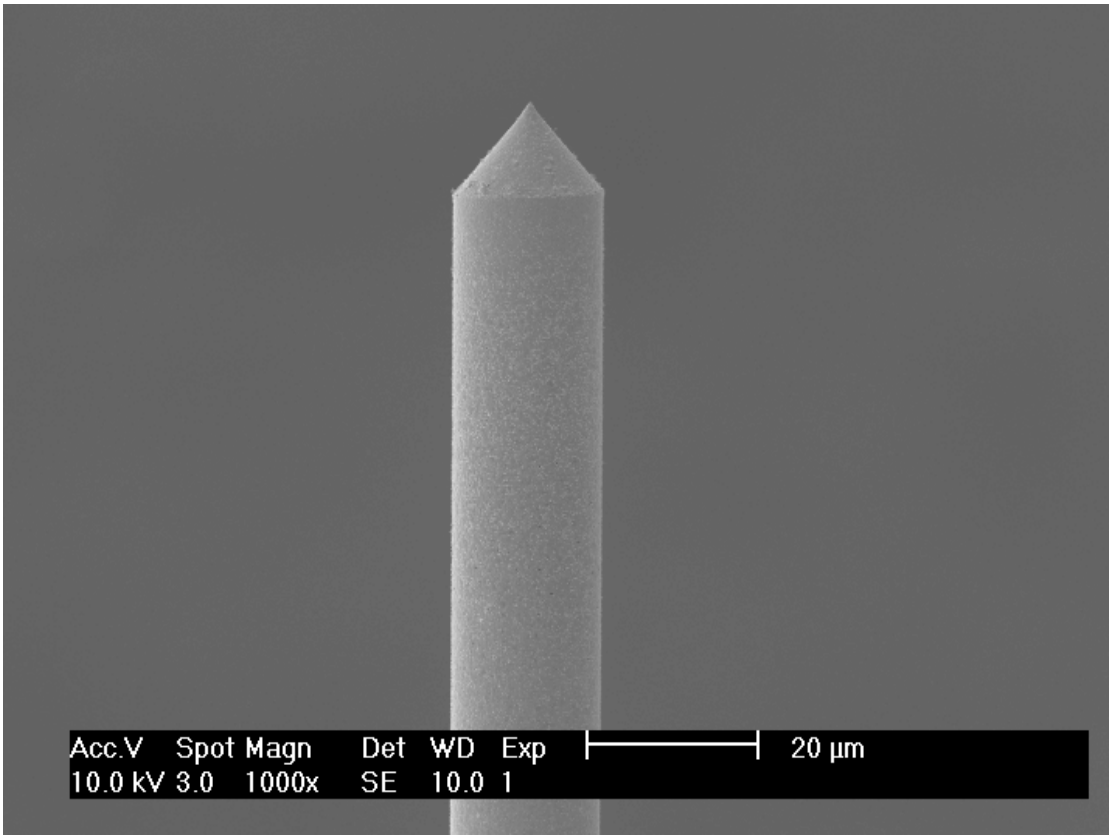

Figure 3.10 SEM image of a gold-coated probe after sputtering of silicon oxide with RF magnetron at 100 W.

We moved the electrode from air into the solution and monitor the current change (schematic shown in Fig. 3.11). The probe scan curve by an electrode insulated by silicon oxide from rf magnetron sputtering is shown in Fig. 3.12. The tip current continued to increase when we dipped it further in the solution. It seems the electrode is not completely insulated. To evaluate how much is the insulation, we compared the experimental curve with a theoretical curve for cylindrical UME.3 In the long-time limit, a practical approximation of the current at a cylindrical UME, reported by Szabo et al.,4 is

$$i_{qss} = \frac{2nFAD_0C_0}{r_0 \ln \tau} \qquad (1)$$

where $\tau = 4D_0t/r_0^2$, i_{qss} is quasi-steady state current because time appears only as an inverse logarithmic function, so that the current declines rather slowly in the long-time limit. As the electrode was kept moving, t at the tip is larger than that in the region which just contacts with the solution.

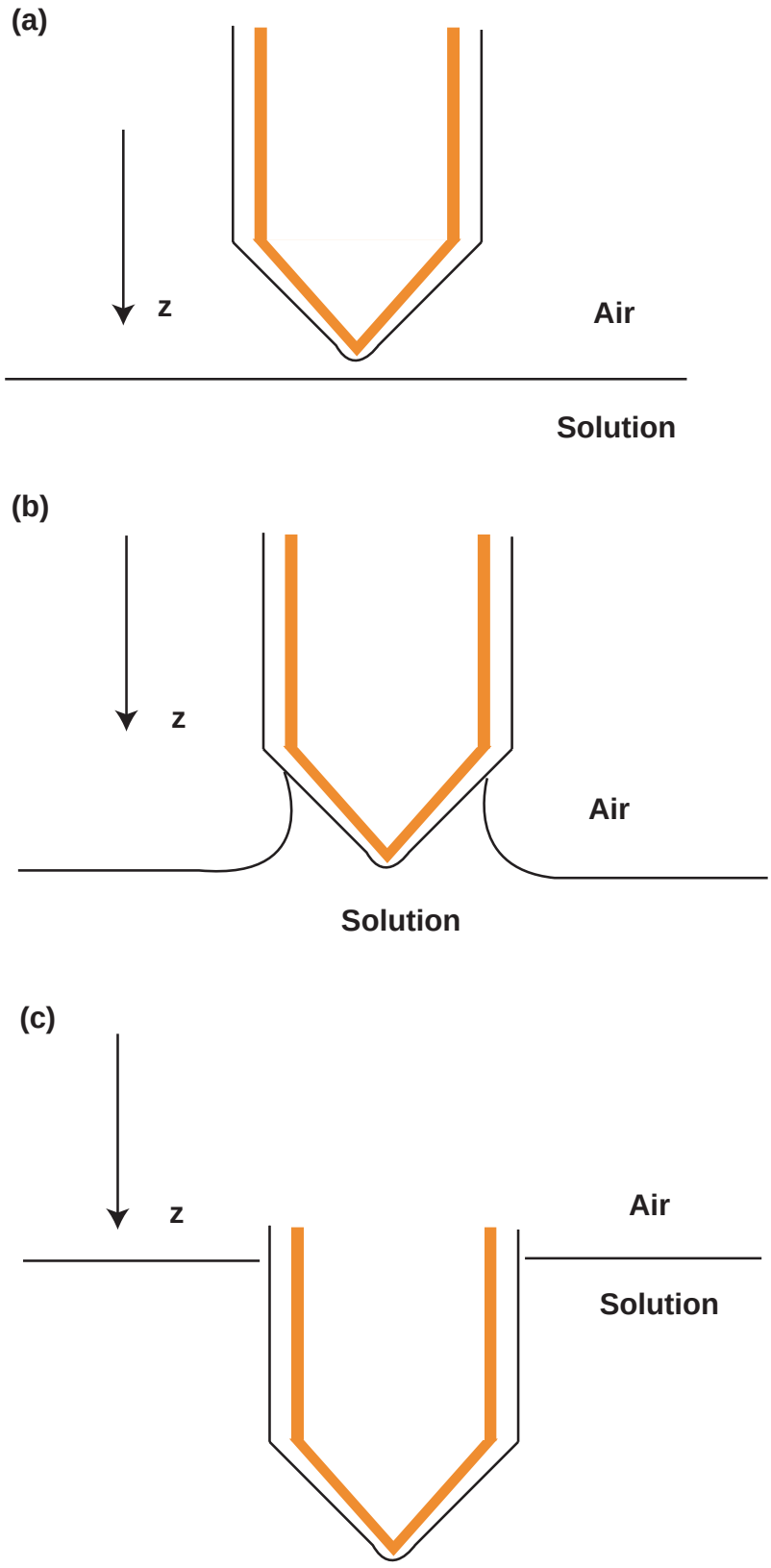

Figure 3.11 Schematic of probe scan

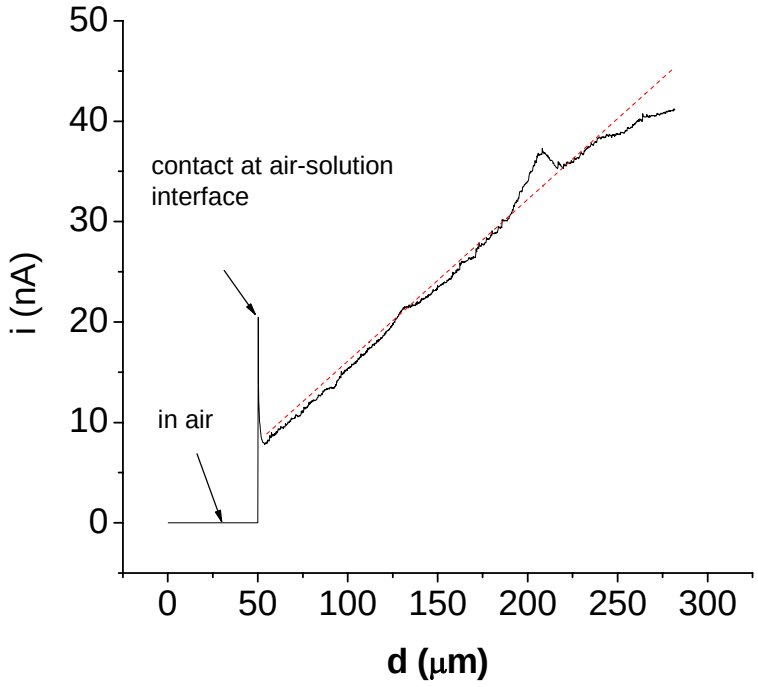

Figure 3.12 Comparison for experimental probe scan curve (solid line) with theoretical one (cylindrical UME, dashed line). Solution contains 1 mM 1,1′-ferrocenedimethanol and 0.1 M KCl.

So we averaged this effect and approximately set *t* as 5 s for theoretical calculation. From Fig.3.12, it seems our electrode behaved like a cylindrical UME which has a completely active surface. Our explanation to this result is as follows: even though we have sputtered silicon oxide on the gold-coated fibers, there is possibility of pinholes, through which electroactive species may access the electrode surface. Those pinholes behave like microelectrode arrays. At short time scales, when diffusion layer thickness is smaller compared to the size of the pinhole, each spot generates its own diffusion field (Fig. 3.13a), and the area of the overall diffusion is the sum of individual active spot. At longer time scales, the individual diffusion layer begins to overlap with each other and the separate diffusion fields merge into one single larger field (Fig. 13b),

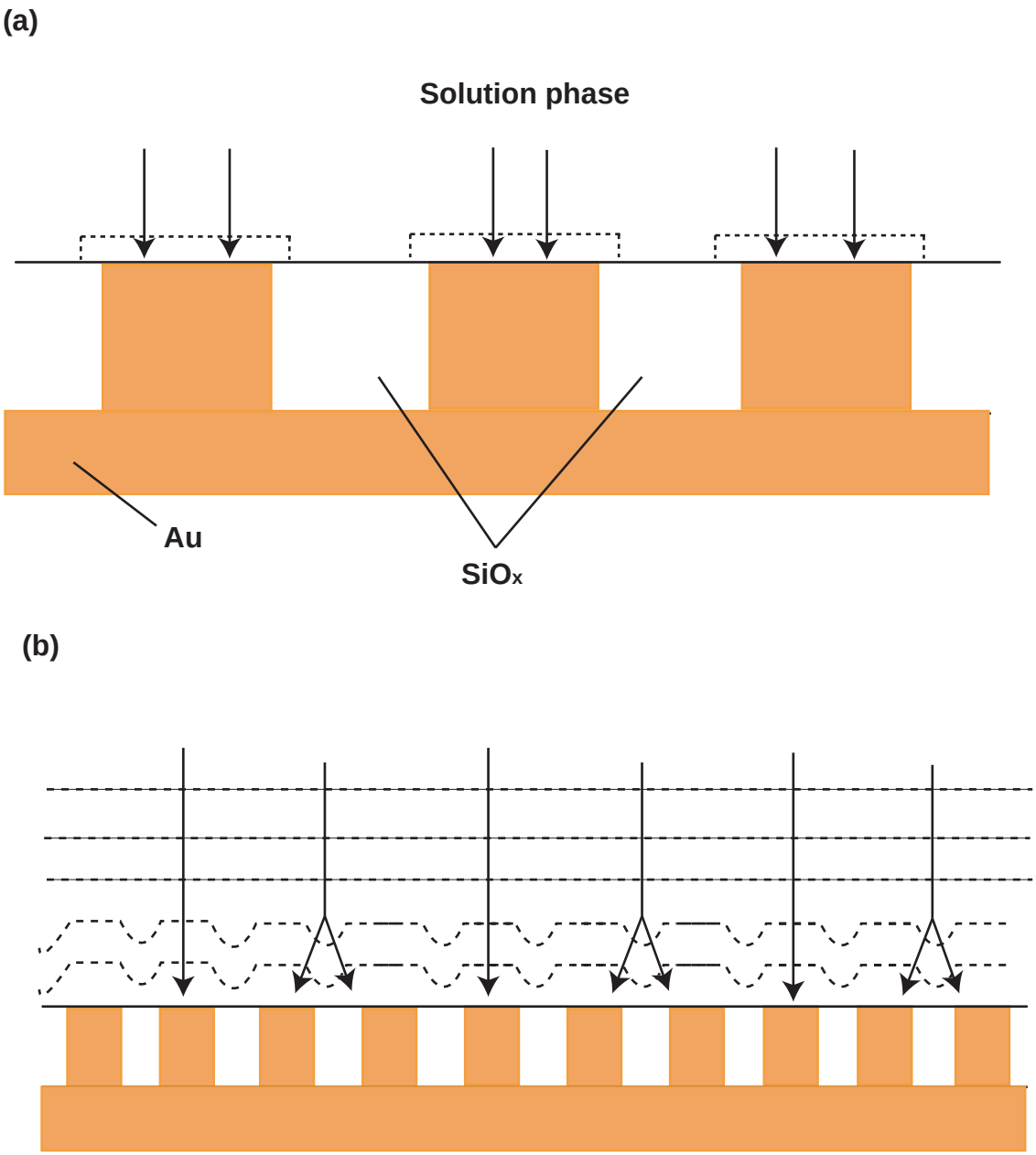

Figure 3.13 Evolution of the diffusion layer at an electrode with pinholes. (a) short time scale (b) long time scale. Dotted lines show surface of equal concentration in the diffusion layer. Arrows indicate concentration gradient driving the flux toward the electrode surface.

again exhibiting linear diffusion and have an area equal to the geometric area of the entire array, even including that of the insulating zones between pinholes. In our case, the diffusion layer thickness ($\sqrt{2Dt}$) at pinholes in 5 s is 83 μm, which should be much larger than the size of the pinhole. Hence, it is reasonable that the silicon oxide sputter-coated electrode behaved like a cylinder one with totally active surface because of pinhole effect. Therefore, optimization of sputtering condition needs further attention.

3.5 CONCLUSION

In order to make nano-electrode under 200 nm in radius, we tried several approaches: FIB milling with electrophoretic paint insulations indicates the size limiting factor is the electrophoretic paint procedure, even though FIB has very good capacity in modifying the size and geometry of probes with nanometer precision and electrophoretic paint technique produces good insulation. Sputtering silicon oxide seems a good option for insulation and the optimization of sputtering condition is still under investigation.

3.6 REFERENCES

(1) Watkins, J. J.; Chen, J. Y.; White, H. S.; Abruna, H. D.; Maisonhaute, E.; Amatore, C. *Analytical Chemistry* **2003**, *75*, 3962-3971.

(2) Melngailis, J. *Journal of Vacuum Science & Technology, B: Microelectronics and Nanometer Structures* **1987**, *5*, 469-495.

(3) Bard, A. J.; Faulkner, L. R. *Electrochemical Methods: Fundamentals and Applications*, 1980.

(4) Szabo, A.; Cope, D. K.; Tallman, D. E.; Kovach, P. M.; Wightman, R. M. *Journal of Electroanalytical Chemistry* **1987**, *217*, 417.

(5) Reyntjens, S.; Puers, R. *Journal of Micromechanics and Microengineering* **2001**, *11*, 287-300.

(6) Kovacs, G. T. A. *Micromachined Transducers Sourcebook*; Tom Casson, 1998.

APPENDIX A

PRINCIPLE OF FIB

A basic setup of a FIB ion column is shown in Fig. I. The principle of operation of FIB is similar to that of SEM, with the major difference being the use of a gallium ion (Ga^+) beam instead of an electron beam. The ion beam is generated from a liquid-metal ion source (LMIS) by the application of a strong electric field. And this electric field causes the emission of positively charged ions from liquid gallium, which is formed on the tip of a tungsten needle. After a first refinement through the spray aperture, the ion beam is condensed in the first electrostatic lens.[5] The upper octopole then corrects the beam for astigmatism. Using variable aperture mechanism, the beam can achieve with desired characteristics: either a “large” beam with high current or a “small” beam with low current. Blanking of the beam is accomplished by the blanking deflectors and aperture, while the lower octopole is used for raster scanning the beam over the sample in a user-defined fashion. In the second electrostatic lens, the beam is focused to a fine spot, enabling a best resolution in the sub 10 nm range. The multichannel plate (MCP) is used to collect secondary particles for imaging.

When energetic ions hit the surface of a solid sample, they lose energy to the electrons as well as atoms of the solid. During FIB imaging, the finely focused ion beam is raster scanned over a substrate, and secondary particles (neutral atoms, ions and electrons) are generated in the sample.[5] As they leave the sample, ions or electrons are collected on a biased detector (a MCP). The detector bias is a positive or a negative voltage, respectively, for collecting secondary electrons or ions.

Besides the imaging feature, the ion beam could also be used to remove material from sample surface and this is called FIB milling. Such feature is achieved by using a high ion

current beam. The result is a physical sputtering of sample material, leaving an etched shape by scanning the beam over the substrate.

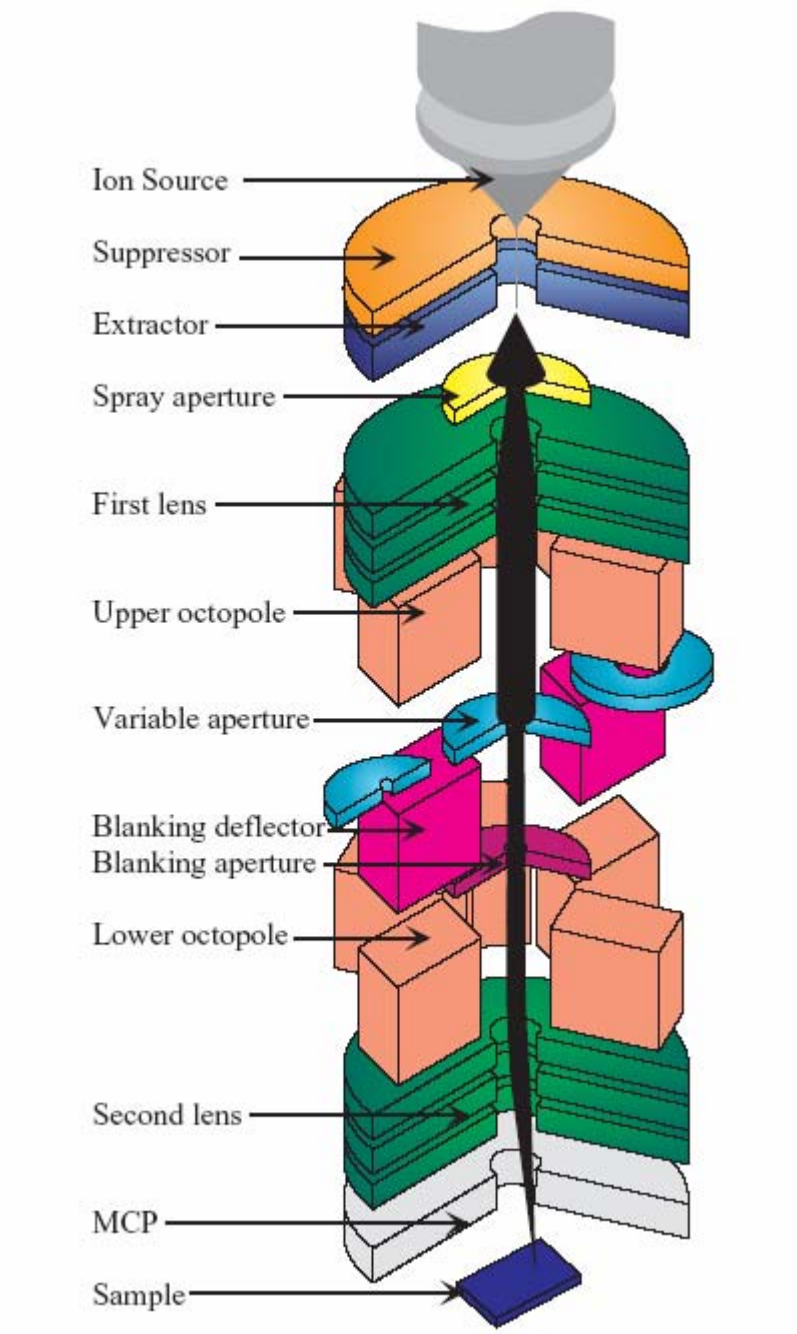

Figure I Schematic of a FIB ion column[5]

APPENDIX B

PRINCIPLE OF SPUTTERING

In sputtering deposition, inert ions (Ar^+) out of a plasma are accelerated using direct current (DC) or radio frequency (RF) potentials through a potential gradient so that they bombard a target, generating ejected cluster of target material and secondary electrons from the recoil of their incident momentum.[6] These secondary electrons cause a further ionization of the inert gas. Through momentum transfer, atoms near the surface of the target become volatile and are transported as a vapor, forming a film on a substrate through deposition. The resulting film properties can be controlled by adjusting sputter parameters such as power, chamber pressure, etc.

4.0 FUTURE WORK

4.1 OPTIMIZATION OF SIOX COATING

As mentioned in Chapter 3, the sputtering condition for silicon oxide on gold-coated fibers are still under adjustment. Many parameters need to be optimized such as chamber pressure, power, coating time, etc. In the near future, we plan to optimize such parameters and wish to obtain continuous and homogeneous coating of SiO_x. After obtaining good quality of SiO_x coating, we can then adjust the thickness of silicon oxide layer to make it suitable for nano-electrode fabrication.

Another option for silicon oxide coating is to use plasma-enhanced chemical vapor deposition (PECVD), which can control the stress at will and has the lowest coating temperature among a number of coating techniques.

4.2 OXYGEN TRANSFER AT WATER/FLUOROCARBON INTERFACE BY SECM

Fluorocarbon, an oxygen carrier, can be used as blood substitute. Therefore, to understand the oxygen transfer at water/fluorocarbon is of fundamental importance. There is no such report on the kinetics measurements of oxygen transfer in above system. With the SECM nano-probes we proposed, it is possible for us to study that system, because if the tip is small enough the whole process is limited by the oxygen transfer across the interface, by which the rate constant can be extracted from comparing SECM approach curve with theoretical one. Meanwhile, such soft interface can be used to determine the electrode geometry without breaking the tiny tip.

4.3 COMBINED SECM/OPTICAL MICROSCOPY

The template we used to fabricate SECM tips is the optical fiber, which is suitable for optical measurements. Bard and co-workers have already succeeded in combining SECM and optical microscopy by using a pulled optical fiber with electrophoretic insulation.[1, 2] The smallest tip they prepared is a ring electrode with ~ 1μm as outer ring diameter. Our goal is to make a ring electrode with the scheme we proposed in chapter 3 at an even smaller dimension, which means a higher spatial resolution, and use it to probe the chemical and optical properties simultaneously on a biological membrane such as nuclear envelope.

4.4 REFERENCES

(1) Lee, Y.; Bard, A. J. *Analytical Chemistry* **2002**, *74*, 3626-3633.

(2) Lee, Y.; Ding, Z. F.; Bard, A. J. *Analytical Chemistry* **2002**, *74*, 3634-3643.